



# Analysis of terrestrial thermospheric $N_2$ $c'_4 \ ^1\Sigma_u^+(0) \sim b' \ ^1\Sigma_u^+(1) - X \ ^1\Sigma_g^+$ dayglow emission observed by the Far Ultraviolet Spectroscopic Explorer

Xianming Liu,<sup>1</sup> Alan N. Heays,<sup>2</sup> Donald E. Shemansky,<sup>1</sup> Brenton R. Lewis,<sup>2</sup> and Paul D. Feldman<sup>3</sup>

Received 12 May 2008; revised 14 January 2009; accepted 2 February 2009; published 10 April 2009.

[1] Terrestrial thermospheric dayglow emission from the coupled and overlapping  $c'_4 \ ^1\Sigma_u^+(0)$  and  $b' \ ^1\Sigma_u^+(1)$  levels of molecular nitrogen, observed by the Far Ultraviolet Spectroscopic Explorer, is analyzed with the aid of a coupled channels quantum mechanical model of  $N_2$  spectroscopy and predissociation dynamics. Model emission spectra for the mixed  $c'_4 \ ^1\Sigma_u^+(0) \sim b' \ ^1\Sigma_u^+(1) - X \ ^1\Sigma_g^+(v_i = 2, 6-9)$  transitions, calculated for the case of excitation by photoelectron impact, are in excellent agreement with the observations. While the principal excitation mechanism for  $N_2$  in the thermosphere is photoelectron impact, evidence is also found in other transitions of resonant fluorescence, induced by lines in the solar atomic hydrogen Lyman series, atomic oxygen transitions, and other  $N_2$  bands. The observed emission rate of the  $c'_4 \ ^1\Sigma_u^+(0) \sim b' \ ^1\Sigma_u^+(1) - X \ ^1\Sigma_g^+(0)$  band is  $\sim 1\%$  of that inferred from the emission rates to  $X \ ^1\Sigma_g^+(v_i > 2)$  levels. A qualitative explanation is given for the drastically reduced intensity and band shape distortion observed in the  $c'_4 \ ^1\Sigma_u^+(0) - X \ ^1\Sigma_g^+(0)$  emission band. Estimates of the total electron excitation rates for the nominal  $b' \ ^1\Sigma_u^+(1)$  and  $c'_4 \ ^1\Sigma_u^+(0)$  levels are determined from the spectrum by extrapolating the model through regions containing unmeasured and/or resonantly absorbed bands.

**Citation:** Liu, X., A. N. Heays, D. E. Shemansky, B. R. Lewis, and P. D. Feldman (2009), Analysis of terrestrial thermospheric  $N_2$   $c'_4 \ ^1\Sigma_u^+(0) \sim b' \ ^1\Sigma_u^+(1) - X \ ^1\Sigma_g^+$  dayglow emission observed by the Far Ultraviolet Spectroscopic Explorer, *J. Geophys. Res.*, *114*, D07304, doi:10.1029/2008JD010403.

## 1. Introduction

[2] Molecular nitrogen is the major component of the atmospheres of the Earth, Titan and Triton.  $N_2$  airglow emissions have been observed from the Earth [Morrison *et al.*, 1990; Meier, 1991; Feldman *et al.*, 2001; Strickland *et al.*, 2004a, 2004b; Bishop *et al.*, 2007], Mars [Kransnopolsky and Feldman, 2002], and planetary satellites [Broadfoot *et al.*, 1989; Liu *et al.*, 2005a; Ajello *et al.*, 2007]. The interpretation of these observations has contributed significantly to our understanding of planetary atmospheric composition and thermal structure.

[3]  $N_2$  dayglow in the vacuum ultraviolet (VUV) region occurs primarily as emission in the lowest dipole-allowed band systems, involving transitions from excited singlet ungerade states in the extreme ultraviolet (EUV) region to the extensive vibrational manifold of the ground state,  $X \ ^1\Sigma_g^+$ .  $N_2$ , stimulated by solar radiation, undergoes a complex chain

of reactions. Since the total ionization oscillator strength of  $N_2$  is  $\sim 12.4$ , much larger than the oscillator strength for neutral transitions,  $\sim 1.6$  [Berkowitz, 2002],  $N_2$  in the thermosphere is primarily ionized by the EUV solar photons, producing  $N_2^+$ ,  $N^+ + N$ ,  $N^+ + N^+$ , and photoelectrons. Therefore, excitation of  $N_2$  to the singlet ungerade states by photoelectron impact provides the principal dayglow excitation mechanism, although resonant excitation by solar radiation (D. E. Shemansky *et al.*, Resonant photoexcitation of  $N_2$  by the solar H Lyman series at high altitudes in the Earth and Titan atmospheres, manuscript in preparation, 2009) and, in limited cases, by nearly coincident, strong  $N_2$  EUV emission via multiple scattering [Stevens *et al.*, 1994], also take place. Predissociation, and spontaneous emission to the singlet gerade states (predominantly  $X \ ^1\Sigma_g^+$ ), are the two primary decay mechanisms for the excited states of  $N_2$ . Thus, realistic interpretation and modeling of the  $N_2$  atmospheric dayglow requires knowledge of both photoelectron- and photon-induced excitation processes, together with radiative and nonradiative decay processes, including accurate and comprehensive information on line positions, oscillator strengths, and predissociation rates.

[4] The singlet ungerade states of  $N_2$  that are dipole-connected to the ground state comprise the  $b' \ ^1\Sigma_u^+$  and  $b \ ^1\Pi_u$  valence states, and the  $np\sigma_u \ c'_{n+1} \ ^1\Sigma_u^+$ ,  $np\pi_u \ c_n \ ^1\Pi_u$ , and  $ns\sigma_g \ o_n \ ^1\Pi_u$  Rydberg series, where  $n$  is the principal

<sup>1</sup>Planetary and Space Science Division, Space Environment Technologies, Pasadena, California, USA.

<sup>2</sup>Research School of Physical Sciences and Engineering, Australian National University, Canberra, ACT, Australia.

<sup>3</sup>Department of Physics and Astronomy, Johns Hopkins University, Baltimore, Maryland, USA.

quantum number. Many experimental and theoretical investigations have shown that strong coupling among the ungerade states of like symmetry results in major energy level and intensity perturbations. Furthermore, many of the excited levels are significantly predissociated. In a semi-empirical study of the coupled states, *Stahel et al.* [1983] demonstrated that the dominant perturbative effect is homogeneous electronic interaction within the  $^1\Sigma_u^+$  and  $^1\Pi_u$  manifolds, primarily of the Rydberg-valence type. *Spelsberg and Meyer* [2001] carried out ab initio calculations on the six lowest members of the  $^1\Sigma_u^+$  and  $^1\Pi_u$  manifolds by introducing internuclear distance ( $R$ )-dependent couplings and transition moments, adjusted to achieve excellent agreement with experimental results. *Carroll and Yoshino* [1972] analyzed the rotational interaction between the  $c'_{n+1}$   $^1\Sigma_u^+$  and  $c_n$   $^1\Pi_u$  series using L-uncoupling theory. Many other investigators [*Helm et al.*, 1993; *Edwards et al.*, 1995; *Ubachs et al.*, 2001; *Sprengers et al.*, 2003] also extended the work of *Stahel et al.* [1983] by including these Rydberg  $p$  complex  $^1\Sigma_u^+ \sim ^1\Pi_u$  heterogeneous interactions. More recently, *Lewis et al.* [2005a, 2005b] and *Haverd et al.* [2005] considered additional spin-orbit interactions between the singlet and triplet  $\Pi_u$  states within a coupled channel Schrödinger equation (CSE) model that has succeeded in explaining quantitatively the  $N_2$  predissociation mechanism for the first time.

[5] The strong coupling among the singlet ungerade levels presents two problems for the interpretation of any  $N_2$  VUV emission spectra, especially those taken at high resolution. First, the strong interaction leads to very significant effective rotational ( $J$ ) dependence of the transition dipole matrix elements. Both experimental [*Stark et al.*, 2000, 2005] and theoretical [*Haverd et al.*, 2005] investigations have noted vibronic band oscillator strengths that vary erratically with  $J$ . Furthermore, the  $P$ ,  $Q$ , and  $R$  branch oscillator strength ratios for many bands deviate significantly from simple Hönl-London factor predictions [*Stark et al.*, 2000, 2005; *Haverd et al.*, 2005; *Liu and Shemansky*, 2006]. Thus, neither the excitation rate to, nor the spontaneous emission rate from, a singlet ungerade level can be estimated reliably from a constant vibronic band oscillator strength partitioned by Hönl-London factors. Another problem arising from the strong coupling is large rotational dependence of the predissociation yield, as demonstrated in several experimental [*Helm et al.*, 1993; *Helm and Cosby*, 1989; *Walter et al.*, 1993, 1994, 2000; *Liu et al.*, 2005b; *Ubachs*, 1997; *Ubachs et al.*, 2001; *Sprengers et al.*, 2004a, 2004b, 2005a, 2005b; *Sprengers and Ubachs*, 2006] and theoretical [*Lewis et al.*, 2005a, 2005b; *Haverd et al.*, 2005] studies. This strong  $J$  dependence of the predissociation yield imparts a temperature dependence to even low-resolution emission cross sections. The temperature of  $N_2$  in the thermosphere, while often unknown, is certainly greater than the room temperature conditions under which most laboratory spectra are measured. Thus, laboratory emission cross sections cannot be used immediately in a model of  $N_2$  dayglow emission, unless the thermospheric temperature has been well matched. In view of these difficulties, accurate modeling of  $N_2$  dayglow is best achieved by employing a physically based model with predictive capabilities, such as the CSE model, which provides line positions, oscillator strengths, and predissociation widths simultaneously.

[6] The Carroll-Yoshino  $c'_4$   $^1\Sigma_u^+ - X^1\Sigma_g^+$  band system appears prominently in the Far Ultraviolet Spectroscopic Explorer (FUSE) observations [*Feldman et al.*, 2001; *Bishop et al.*, 2007]. Emission from the  $c'_4$   $^1\Sigma_u^+(0)$  level is particularly interesting because the  $c'_4$   $^1\Sigma_u^+(0) - X^1\Sigma_g^+(0)$  transition has been found to be only a weak feature in dayglow emission [*Morrison et al.*, 1990], even though it has the largest oscillator strength of any  $N_2$  band in the EUV region and is the strongest emission feature observed in the laboratory [*Ajello et al.*, 1989]. *Stevens et al.* [1994] attributed this weakness in dayglow emission to multiple scattering and predissociation of the  $c'_4$   $^1\Sigma_u^+(0)$  level. They also found the  $c'_4$   $^1\Sigma_u^+(0) - X^1\Sigma_g^+(1)$  band emission, which is the second-strongest emission channel from  $c'_4$   $^1\Sigma_u^+(0)$  in the absence of multiple scattering, to be attenuated by the nearly coincident and highly predissociative  $b^1\Pi_u(2) - X^1\Sigma_g^+(0)$  transition. Because the (diabatic) Franck-Condon factors for the  $c'_4$   $^1\Sigma_u^+(0) - X^1\Sigma_g^+(v_i)$  bands decrease rapidly with  $v_i$  [*Whang et al.*, 1996], it was expected that the dayglow emission to  $v_i > 1$  levels would be very weak. However, a recent analysis of the FUSE spectra by *Bishop et al.* [2007] has found bright  $c'_4$   $^1\Sigma_u^+(0) - X^1\Sigma_g^+(6-9)$  emission. This strength has been explained by *Liu et al.* [2008] as the result of the homogeneous coupling of  $c'_4$   $^1\Sigma_u^+(0)$  to  $b'^1\Sigma_u^+(1)$ , which has a crossing rotational term series and much larger Franck-Condon factors for transitions to the vibrationally excited ground state. In fact, because of this coupling and the overlap of emission lines, the  $c'_4$   $^1\Sigma_u^+(0) - X^1\Sigma_g^+(v_i)$  features referred to by *Bishop et al.* [2007] might more appropriately be labeled as the coupled  $c'_4$   $^1\Sigma_u^+(0) \sim b'^1\Sigma_u^+(1) - X^1\Sigma_g^+(v_i)$  emission bands.

[7] *Liu et al.* [2008] have recently performed a joint experimental and theoretical study of the  $c'_4$   $^1\Sigma_u^+(0) - X^1\Sigma_g^+$  band system and obtained consistent oscillator strengths and predissociation rates. The work presented here is an extension and application of those results, comprising an analysis of FUSE observations relevant to the  $c'_4$   $^1\Sigma_u^+(0) \sim b'^1\Sigma_u^+(1) - X^1\Sigma_g^+(v_i = 0-9)$  transitions. This analysis is nontrivial since the  $N_2$  emission spectrum is congested and it was found necessary to extend the calculations to take account of overlapping emissions from other excited levels. The present analysis achieves very good agreement between calculated and observed spectra and leads to the determination of reliable emission and excitation rates for the nominal  $b'^1\Sigma_u^+(1)$  and  $c'_4$   $^1\Sigma_u^+(0)$  levels.

[8] Other  $N_2$  features are found to appear prominently in the terrestrial dayglow, originating from upper state levels  $c'_4$   $^1\Sigma_u^+(v_j = 3, 4, 6)$ ,  $b^1\Pi_u(v_j = 1)$ , and  $b'^1\Sigma_u^+(v_j = 4, 7, 9)$  [*Feldman et al.*, 2001; *Bishop et al.*, 2007]. While the present modeling of some of these features (i.e.,  $c'_4$   $^1\Sigma_u^+(3-6)$ ), based on photoelectron-impact-induced emission, contains significant uncertainties, there are, nevertheless, strong indications of an additional excitation channel, i.e., resonant solar excitation of  $N_2$  by a number of solar lines in the hydrogen Lyman series. Some evidence will be presented here, with additional details given in a paper by *Shemansky et al.* (manuscript in preparation, 2009), in which observed absorption of the solar spectrum by  $N_2$  is reported.

## 2. Observations

[9] Observations of the illuminated disk of the Earth were obtained during commissioning of the FUSE satellite in

September 1999. Details of the viewing geometry and references to the spacecraft instrumentation have been given by *Feldman et al.* [2001], who presented an atlas of the airglow emissions obtained through the medium-resolution (MDRS) aperture. The effective spectral resolution of the atlas, which spanned from 905 to 1184 Å, was ~0.07 Å full width at half maximum (FWHM). The low-resolution (LWRS) aperture, which has 11.25× the throughput of the MDRS aperture and gives an effective spectral resolution of ~0.4 Å FWHM, was used to derive limb profiles of the strongest emissions. Subsequently, *Bishop et al.* [2007] used the LWRS data in their investigation of the relatively weak Carroll-Yoshino bands of N<sub>2</sub>. For their analysis, the spectra were reprocessed through the calibration pipeline using version 2.2.1 of CalFUSE. Nevertheless, they noted residual wavelength shifts that were corrected manually with the aid of atomic airglow emissions. The longest-wavelength data (λ > 1130 Å), covered by the LiF1b channel, was also known to suffer from a problem (called the “worm”), resulting from a shadow caused by a repeller grid that rendered the extended source calibration suspect.

[10] In preparation for the final archiving of the FUSE data, additional enhancements to the pipeline were incorporated into version 3.2 of CalFUSE [*Dixon et al.*, 2007]. Of relevance to the data of interest here, these included temperature-dependent wavelength corrections, a more complete evaluation of detector background, and a correction for the “worm” in long-wavelength extended source extractions. The LWRS data presented in this paper utilize this final calibration. In comparison with the data discussed by *Bishop et al.* [2007], the brightnesses of the long-wavelength Carroll-Yoshino (0,7), (0,8), and (0,9) bands are reduced by 8%, 14%, and 30%, respectively. At shorter wavelengths, the differences between the two data sets are <5%. The overall absolute flux calibration, based on standard stars, and adjusted for the date of observation, is accurate to better than 5% [*Dixon et al.*, 2007].

[11] The LWRS data analyzed in the present work cover the 904–993, 987–1083, and 1094–1188 Å regions. Uncertainties in the observed N<sub>2</sub> emission intensities used for comparison with the model are determined primarily by variations in viewing angle and solar activity during the observations. The intensities of O I features in different scans of the 988–992 Å region vary by up to 10%. In the case of the weaker N<sub>2</sub> features, the estimated uncertainties range from 10 to 15%.

### 3. Theory

#### 3.1. Electron-Impact-Induced Emission

[12] The volumetric photon emission rate  $I$  resulting from electron impact excitation is proportional to the excitation rate and the emission branching ratio:

$$I(v_j, v_i; J_j, J_i) = g(v_j; J_j) \frac{A_r(v_j, v_i; J_j, J_i)}{A_r(v_j; J_j) + A_{nr}(v_j; J_j)}, \quad (1)$$

where  $v$  and  $J$  are the vibrational and rotational quantum numbers, respectively,  $A_r(v_j, v_i; J_j, J_i)$  is the Einstein spontaneous transition probability for emission from level  $(v_j; J_j)$  to level  $(v_i; J_i)$ , and  $A_r(v_j; J_j) = \sum_i A_r(v_j, v_i; J_j, J_i)$

and  $A_{nr}(v_j; J_j)$  are the total radiative and nonradiative (in the present case, predissociation only) transition probabilities, respectively, for level  $(v_j; J_j)$ . In the present paper, the subscript index  $i$  always refers to the X<sup>1</sup>Σ<sub>g</sub><sup>+</sup> state, while index  $j$  refers to the excited singlet ungerade states.

[13] The excitation rate  $g(v_j; J_j)$  is proportional to the number density of N<sub>2</sub> in the initial level,  $N(v_i; J_i)$ , the excitation cross section  $\sigma(v_i, v_j; J_i, J_j)$ , and the electron flux  $F_e$ :

$$g(v_j; J_j) = F_e \sum_i N(v_i; J_i) \sigma(v_i, v_j; J_i, J_j). \quad (2)$$

[14] For a dipole-allowed rovibronic excitation from electronic state  $i$  to state  $j$ , the excitation cross section, based on the modified Born approximation, is given by [*Shemansky et al.*, 1985]:

$$\begin{aligned} \frac{\sigma(v_i, v_j; J_i, J_j)}{\pi a_0^2} &= 4f(v_i, v_j; J_i, J_j) \frac{Ry Ry}{E_{ij} E} \left[ \frac{C_0}{C_7} \left( \frac{1}{X^2} - \frac{1}{X^3} \right) \right. \\ &\quad + \sum_{m=1}^4 \frac{C_m}{C_7} (X-1) \exp(-mC_8 X) \\ &\quad \left. + \frac{C_5}{C_7} + \frac{C_6}{C_7 X} + \ln(X) \right], \quad (3) \end{aligned}$$

$$\text{where } C_7 = \frac{4\pi a_0^2 (2J_i + 1) Ry}{E_{ij}} f(v_i, v_j; J_i, J_j), \quad (4)$$

and  $a_0$  and  $Ry$  are the Bohr radius and Rydberg constant, respectively,  $f(v_i, v_j; J_i, J_j)$  is the absorption oscillator strength,  $E_{ij}$  is the transition energy from  $(v_i; J_i)$  to  $(v_j; J_j)$ ,  $E$  is the impact energy, and  $X = E/E_{ij}$  is the dimensionless electron energy. The collision strength coefficients  $C_k/C_7$  ( $k = 0 - 6$ ) and  $C_8$  reflect atomic or molecular electronic properties and are usually assumed to be dependent on electronic state, but independent of rotation and vibration. These have been measured experimentally for the c'<sub>4</sub><sup>1</sup>Σ<sub>u</sub><sup>+</sup> and b'<sup>1</sup>Π<sub>u</sub> – X<sup>1</sup>Σ<sub>g</sub><sup>+</sup> band systems by *Ajello et al.* [1989] and *James et al.* [1990], respectively. The c'<sub>4</sub><sup>1</sup>Σ<sub>u</sub><sup>+</sup> – X<sup>1</sup>Σ<sub>g</sub><sup>+</sup> collision strength parameters are, in the absence of any direct measurements, assumed to be also applicable to b'<sup>1</sup>Σ<sub>u</sub><sup>+</sup> – X<sup>1</sup>Σ<sub>g</sub><sup>+</sup> transitions. Similarly, the b'<sup>1</sup>Π<sub>u</sub> – X<sup>1</sup>Σ<sub>g</sub><sup>+</sup> parameters are extended to the c<sub>3</sub><sup>1</sup>Π<sub>u</sub> – X<sup>1</sup>Σ<sub>g</sub><sup>+</sup> system. An alternative, and perhaps better, assumption would be to take the b'<sup>1</sup>Π<sub>u</sub> – X<sup>1</sup>Σ<sub>g</sub><sup>+</sup> and b'<sup>1</sup>Σ<sub>u</sub><sup>+</sup> – X<sup>1</sup>Σ<sub>g</sub><sup>+</sup> (valence) parameters to be the same, and the c<sub>3</sub><sup>1</sup>Π<sub>u</sub> – X<sup>1</sup>Σ<sub>g</sub><sup>+</sup> and c'<sub>4</sub><sup>1</sup>Σ<sub>u</sub><sup>+</sup> – X<sup>1</sup>Σ<sub>g</sub><sup>+</sup> (Rydberg) parameters to be the same. However, while these assumptions can lead to uncertainties in the  $g$  values used in equation (1) for the b'<sup>1</sup>Σ<sub>u</sub><sup>+</sup> – X<sup>1</sup>Σ<sub>g</sub><sup>+</sup> and c<sub>3</sub><sup>1</sup>Π<sub>u</sub> – X<sup>1</sup>Σ<sub>g</sub><sup>+</sup> transitions, these uncertainties are unlikely to be important in the present study, which focuses principally on the c'<sub>4</sub><sup>1</sup>Σ<sub>u</sub><sup>+</sup>(0) – X<sup>1</sup>Σ<sub>g</sub><sup>+</sup>(v<sub>i</sub>) transitions. Furthermore, we note that electron-energy-dependent non-Franck-Condon effects in the relative vibrational excitation cross sections for a given electronic transition, similar to those discussed in detail for O<sub>2</sub> [*Lewis et al.*, 2001], are likely to occur also for N<sub>2</sub> [*Joyez et al.*, 1973]. While this is not relevant to the excitation of the fixed upper state vibrational levels considered here, similar interference effects may influence the intensity sharing in emission between the c'<sub>4</sub><sup>1</sup>Σ<sub>u</sub><sup>+</sup>(0) and b'<sup>1</sup>Σ<sub>u</sub><sup>+</sup>(1) decay channels,

particularly for the higher- $v_i$  bands where the c'<sub>4</sub><sup>1</sup>Σ<sub>u</sub><sup>+</sup>(0) emission is not completely dominant.

[15] The line transition probability  $A_i(v_j, v_i; J_j, J_i)$  of equation (1), in s<sup>-1</sup>, is related to line oscillator strength  $f(v_i, v_j; J_i, J_j)$  of equation (3) by [Abgrall and Roueff, 2006]:

$$A(v_j, v_i; J_j, J_i) = 0.667 \frac{(2J_i + 1)}{(2J_j + 1)} \nu^2(v_i, v_j; J_i, J_j) f(v_i, v_j; J_i, J_j), \quad (5)$$

where  $\nu(v_i, v_j; J_i, J_j)$  is in cm<sup>-1</sup>.

### 3.2. Coupled Channels Calculations

[16] A CSE model of N<sub>2</sub> structure and predissociation dynamics is employed here to describe the dipole-allowed spectrum, providing transition energies, oscillator strengths, and predissociation line widths, at the rovibronic level, for application to the current problem of modeling the N<sub>2</sub> dayglow emissions. The primary advantage of a CSE treatment is the implicit inclusion of all vibrational levels as well as the dissociation continua of the coupled excited molecular electronic states. This is critical for an accurate account of N<sub>2</sub> structure, where strong perturbations span many vibrational levels. Being physically based, the model is able to interpolate and extrapolate realistically into the regions where experimental spectroscopic data are unavailable. The particular CSE model used is an extension of the work of Lewis et al. [2005a] and Haverd et al. [2005], having been described previously by Liu et al. [2008].

[17] Specifically, the model excited state manifold comprises the  $b$ ,  $c_3$ , and  $o_3$  <sup>1</sup>Π<sub>u</sub>, the  $b'$ ,  $c'_4$ , and  $c'_5$  <sup>1</sup>Σ<sub>u</sub><sup>+</sup>, and the  $C$ ,  $C'$ ,  $F$ , and  $G$  <sup>3</sup>Π<sub>u</sub> states. Three levels of interactions are included in the model: homogeneous electrostatic interactions among the states within the <sup>1</sup>Π<sub>u</sub>, <sup>1</sup>Σ<sub>u</sub><sup>+</sup>, and <sup>3</sup>Π<sub>u</sub> Rydberg-valence manifolds; homogeneous spin-orbit interactions between the <sup>1</sup>Π<sub>u</sub>, <sup>1</sup>Σ<sub>u</sub><sup>+</sup> and <sup>3</sup>Π<sub>u</sub> manifolds; and heterogeneous L-uncoupling interactions between the <sup>1</sup>Π<sub>u</sub> and <sup>1</sup>Σ<sub>u</sub><sup>+</sup> manifolds. Inclusion of the <sup>3</sup>Π<sub>u</sub> manifold, which contains the unbound  $C'$  state, allows the correct treatment of N<sub>2</sub> predissociation. The indirect mechanism proposed by Lewis et al. [2005a] to explain the predissociation of the lowest <sup>1</sup>Π<sub>u</sub> levels is extended to higher levels, through the inclusion of the  $F$  and  $G$  Rydberg states in the <sup>3</sup>Π<sub>u</sub> manifold [Lewis et al., 2008a], and to the <sup>1</sup>Σ<sub>u</sub><sup>+</sup> levels, by a preliminary consideration of their spin-orbit coupling to the <sup>3</sup>Π<sub>u0</sub> states.

[18] The formalism of the CSE technique has been detailed by van Dishoeck et al. [1984]. The model parameters include the diabatic potential energy curves for each electronic state and the  $R$ -dependent diabatic electronic transition moments for those states that possess dipole-allowed transitions to the X<sup>1</sup>Σ<sub>g</sub><sup>+</sup> ground state of N<sub>2</sub>. The electrostatic interactions between singlet ungerade states of like symmetry are represented by  $R$ -dependent electronic coupling parameters, the L-uncoupling and spin-orbit interactions by  $R$ -independent parameters. All of the  $R$ -dependent parameters associated with the <sup>1</sup>Σ<sub>u</sub><sup>+</sup> and <sup>1</sup>Π<sub>u</sub> states are initialized from the ab initio results of Spelsberg and Meyer [2001], except the transition moment for c'<sub>4</sub><sup>1</sup>Σ<sub>u</sub><sup>+</sup> – X<sup>1</sup>Σ<sub>g</sub><sup>+</sup> which was derived from experimental oscillator strengths over a progression of both upper and lower state vibrational levels, as described by Liu et al. [2008]. All CSE model parameters have been least

squares optimized against a large database of line energies, strengths and widths [Carroll and Collins, 1969; Helm et al., 1993; Helm and Cosby, 1989; Kam et al., 1989; Kawamoto et al., 1997; Levelt and Ubachs, 1992; Lewis et al., 2008a, 2008b; Liu et al., 2008; Ndome et al., 2008; Roncin et al., 1991, 1998, 1999; Smith et al., 2003, see also Harvard-Smithsonian Center for Astrophysics Molecular Database, <http://www.cfa.harvard.edu/amp/ampdata/14n2/eglpdf.html>; Spelsberg and Meyer, 2001; Sprengers, 2006; Sprengers et al., 2003, 2004a, 2004b, 2005a, 2005b; Sprengers and Ubachs, 2006; Stark et al., 1992, 2000, 2005, 2008; Ubachs et al., 2000, 2001; Vieitez et al., 2007, 2008; Yoshino et al., 1975, 1979; Yoshino and Tanaka, 1977].

[19] Model photodissociation spectra are continuous in energy because of the inclusion of unbound states in the coupled equations, enabling the determination of resonance energies, oscillator strengths, and line widths by fitting Fano profiles to the CSE model cross sections. The CSE oscillator strengths are used in equations (3), (4), and (5) to determine the electron excitation rate and the photon emission rates to the ground state vibrational manifold. The predissociative contribution to the total decay rate  $A(v_j; J_j)$  is determined from the CSE model predissociation line width  $\Gamma_{nr}(v_j; J_j)$  using the relation  $A_{nr}(v_j; J_j) = \hbar^{-1} \Gamma_{nr}(v_j; J_j)$ . With  $\Gamma_{nr}(v_j; J_j)$  in cm<sup>-1</sup> FWHM,

$$A_{nr}(v_j; J_j) = 1.88 \times 10^{11} \Gamma_{nr}(v_j; J_j) \text{s}^{-1}. \quad (6)$$

[20] The fitted CSE model ( $v_j, 0$ ) band origins differ by a maximum of a few tenths of a cm<sup>-1</sup> from the experimental database values. In order to ascertain the accuracy of the calculated singlet transition energies over the complete range of rovibrational levels of interest, experimentally determined term values reported by Levelt and Ubachs [1992], Roncin et al. [1998, 1999], Stark et al. [2005], Smith et al. [2003, see also Harvard-Smithsonian Center for Astrophysics Molecular Database, <http://www.cfa.harvard.edu/amp/ampdata/14n2/eglpdf.html>], Yoshino and Tanaka [1977], and Yoshino et al. [1979], as well as Le Roy et al. [2006], for the high  $v_i$  levels of X<sup>1</sup>Σ<sub>g</sub><sup>+</sup>, have been compared with CSE model level energies. The CSE term value residues were found to be no more than 1.4 cm<sup>-1</sup>, whereas in congested regions, measured term values from different experiments can differ by as much as 1 cm<sup>-1</sup>.

[21] The fitted CSE model ( $v_j, 0$ ) band oscillator strengths differ from those in the experimental database by a maximum of ±10%. A more detailed comparison with the rotationally dependent experimental oscillator strengths of Stark et al. [2005, 2008] for  $b - X(0 - 14, 0)$ ,  $c_3 - X(0 - 3, 0)$ ,  $o_3(0 - 3, 0)$ ,  $b' - X(0 - 11, 0)$ , and  $c'_4 - X(0 - 3, 0)$  reveals encouraging detailed agreement at the ±15% level. A similar degree of agreement is expected for higher-energy levels. Because of the lack of experimental data for comparison, there is no opportunity to comprehensively verify the CSE model ( $v_j, v_i > 0$ ) oscillator strengths. However, since the CSE treatment of the coupled excited states has been shown to be valid, it is likely that the ( $v_j, v_i > 0$ ) oscillator strengths will be almost as accurate as those for the ( $v_j, 0$ ) transitions. In particular, of prime relevance to this work, Liu et al. [2008] have demonstrated the ability of the CSE model to predict the relative band intensities of the overlapping and strongly mutually perturbing b'<sup>1</sup>Σ<sub>u</sub><sup>+</sup>(1)- and

$c'_4$   $^1\Sigma_u^+(0) - X^1\Sigma_g^+(0-3)$  emission bands when compared with laboratory electron-excited spectra. This result included the correct reproduction of non-Hönl-London line oscillator strengths and  $P/R$  branch interference effects due to coupling with the  $^1\Pi_u$  manifold.

[22] The modeling of predissociation line widths, which may vary over many orders of magnitude with vibration, rotation, or isotopomer, is significantly more problematic than the modeling of oscillator strengths, since more states and couplings are pertinent, leading to greater uncertainty and less predictability. However, CSE-modeled line widths have been compared successfully with experiment for the  $f$  parity levels of  $b(0-6)$  and  $c_3(0)$  by *Lewis et al.* [2005a]. This reduced model ( $f$  parity only, no  $^1\Sigma_u^+$  states included) reproduced correctly the line width pattern for the  $^{14}N_2$ ,  $^{14}N^{15}N$  and  $^{15}N_2$  isotopomers, as does the present expanded model. In addition, modeled rotationally resolved predissociation level widths for  $b(1, 2-4)$  have been shown to agree well with experiment by *Haverd et al.* [2005] and *Lewis et al.* [2005b]. For further levels where limited measurements are available [*Oertel et al.*, 1982; *Kawamoto et al.*, 1997; *Ubachs*, 1997; *Ubachs et al.*, 2000, 2001; *Sprengers and Ubachs*, 2006; *Stark et al.*, 2008] the calculated predissociation widths are consistent with the experimental lifetimes or widths. The most significant uncertainty in the CSE model predissociation widths relates to the homogeneous part of the broadening in the  $^1\Sigma_u^+$  states, which is difficult to establish because of lack of experimental data for comparison. This limitation affects principally the narrowest rotational levels of the higher  $b'$  and  $c'$  vibrational states.

[23] For the particular excited state levels of interest in the following sections, first we note that the CSE model predissociation widths (and oscillator strengths) have been confirmed to have the correct rotational dependence by comparison between the modeled rotational profile of the  $c'_4$   $^1\Sigma_u^+(v_j = 0) - X^1\Sigma_g^+(v_i = 1-2)$  bands and the high-resolution spectra of *Liu et al.* [2008]. Second, insofar as comparisons are possible, the CSE model predissociative lifetimes for the  $b'(4)$  and  $b'(7)$  levels are consistent with experiment. In the case of  $b'(4)$ , the CSE lifetime decreases from 400 to 75 ps as  $J_j$  increases from 0 to 5, consistent with the average experimental lifetime of  $160 \pm 70$  ps for  $J_j \leq 5$  of *Sprengers and Ubachs* [2006]. Because of a strong perturbation by a crossing  $^3\Pi_u$  level, the CSE lifetime varies irregularly in the range 7–67 ps for  $J_j = 6 - 25$ , in agreement with the rapid broadening observed in photoabsorption spectra [*Stark et al.*, 2005; G. Stark et al., unpublished data, 2009]. In the case of  $b'(7)$ , the CSE predissociative lifetime is in the range 1400–1110 ps, for  $J_j = 0 - 10$ , in satisfactory agreement with the only experimental value,  $930 \pm 140$  ps, which is a total lifetime obtained at the band level by *Oertel et al.* [1982], including both radiative and predissociative components. As  $J_j$  increases from 11 to 21, the CSE lifetime decreases rapidly from 790 to 8 ps, in agreement with the broadening observed in photoabsorption spectra *Stark et al.*, unpublished data, 2009).

#### 4. Analysis

[24] The primary focus of the present work is on the mixed  $c'_4$   $^1\Sigma_u^+(0) \sim b'^1\Sigma_u^+(1) - X^1\Sigma_g^+(v_j)$  transitions. Because of various overlapping transitions involving excited

state levels other than  $c'_4$   $^1\Sigma_u^+(0)$  and  $b'^1\Sigma_u^+(1)$ , the current  $e + N_2$  model also considers the emission from  $b'^1\Sigma_u^+(v_j = 0 - 14)$ ,  $b^1\Pi_u(v_j = 0 - 14)$ ,  $c'_4$   $^1\Sigma_u^+(v_j = 0 - 4)$ , and  $c_3$   $^1\Pi_u(v_j = 0 - 1)$ , for rotational levels up to  $J_j = 30$ .

[25] Before comparison with the FUSE spectrum, the  $e+N_2$  model was checked against laboratory emission spectra obtained at room temperature and 100-eV excitation energy. There were discrepancies for some transitions, e.g., for  $c_3$   $^1\Pi_u - X^1\Sigma_g^+$ , as noted by *Liu et al.* [2008]. Small uniform scalings of those transition intensities were sufficient to make the model accurately reproduce the calibrated experimental spectrum. Responsibility for the observed discrepancies is likely to lie either with the assumed form adopted for the  $b'^1\Sigma_u^+ - X^1\Sigma_g^+$  and  $c_3$   $^1\Pi_u - X^1\Sigma_g^+$  collision strength coefficients described in section 1, or, particularly for some higher-vibrational levels of  $^1\Sigma_u^+$  symmetry, with uncertainties in their CSE-calculated predissociation rates. A specific calibration of the electron excitation/emission model is necessary in order to establish the importance of additional excitation mechanisms, as described in section 5.2, and of overlapping transitions other than those originating from  $c'_4$   $^1\Sigma_u^+(0)$  and  $b'^1\Sigma_u^+(1)$ , as described in section 5.4.

[26] Since the temperature of the terrestrial thermosphere is significantly higher than the laboratory temperature, it is possible that the 300-K calibration will not be completely accurate for analysis of the FUSE spectra. The model  $N_2$  emission spectrum was calculated for various temperatures between 300 and 800 K, and convolved with a Gaussian of 0.4-Å FWHM, before being compared with the FUSE spectrum. Good agreement between the calculated and observed relative intensities within the spectral regions containing the  $c'_4$   $^1\Sigma_u^+(0) \sim b'^1\Sigma_u^+(1) - X^1\Sigma_g^+(v_i = 2 - 9)$  bands was obtained by assuming a temperature of  $500 \pm 50$  K. It is important to note that this is an apparent temperature chosen to give good agreement between the observed and optically thin model spectra for  $v_i = 2 - 9$ . As will be shown in section 5.3, multiple scattering of the  $c'_4$   $^1\Sigma_u^+(0) - X^1\Sigma_g^+(0)$  band and  $J$ -dependent predissociation lead to different intensity patterns for primary and secondary emission. The net result is that the observed relative intensity from the high rotational levels is weaker than that for the primary emission. Thus, the inferred temperature of 500 K likely represents a lower limit of the  $N_2$  temperature in the thermosphere.

[27] The relative intensities of the  $c'_4$   $^1\Sigma_u^+(0) - X^1\Sigma_g^+$  and  $b'^1\Sigma_u^+(1) - X^1\Sigma_g^+$  transitions are not sensitive to excitation energy because their threshold energies are nearly coincident. Thus, it is not possible to determine the photoelectron energy from this source. Nevertheless, in the future, the electron-energy-dependent non-Franck-Condon effects discussed in section 3.1 might provide a means of estimating the dominant photoelectron energy, through the fitting of relative vibrational intensities in transitions from strongly Rydberg-valence mixed excited states in dayglow emission spectra. However, significant laboratory measurements and CSE model development will be necessary before this becomes feasible.

[28] The identification of spectral features from species other than  $N_2$ , mostly atomic and ionic oxygen and nitrogen, were based on two online databases by *Ralchenko et al.* [2007], and P. L. Smith et al. (1995 atomic line data (R. L. Kurucz and B. Bell), Kurucz CD-ROM 23, Smithsonian Astrophysics Observatory, Cambridge, Massachusetts, avail-

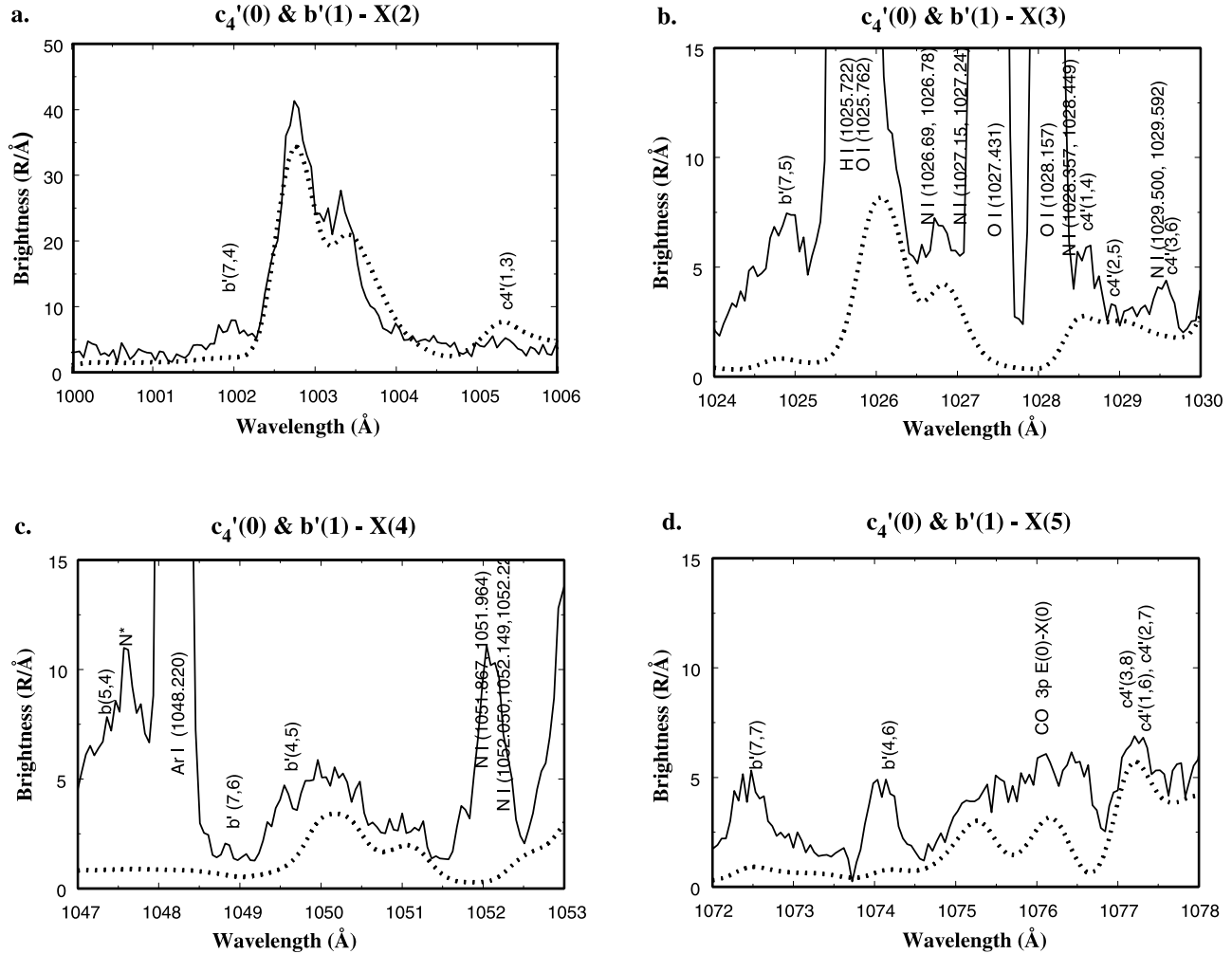


**Figure 1.** Comparison of FUSE observed (solid curves) and model calculated (dotted curves) spectra in the neighborhood of the  $c'_4 \ ^1\Sigma_u^+(0) \sim b' \ ^1\Sigma_u^+(1) - X \ ^1\Sigma_g^+(v_i = 2-5)$  emission bands. The model spectra consider electron impact excitation of  $N_2$  only, assuming a rotational temperature of 500 K and a Gaussian instrument profile with FWHM of 0.4 Å. The approximate wavelength ranges for the less apparent  $v_i = 3, 4,$  and  $5$  bands are 1025.5–1027.6, 1049.6–1051.6, and 1074.5–1076.7 Å, respectively. The spectral peak marked with  $N^*$  at  $\sim 1047.5$  Å appears in 100-eV  $e + N_2$  laboratory spectra but is absent in 20-eV spectra, indicating that it is due to emission from either atomic or ionic nitrogen. Resonant excitation of  $N_2$   $b' \ ^1\Sigma_u^+(4)$  and  $b' \ ^1\Sigma_u^+(7)$  levels by the solar H Lyman series locally raises the corresponding intensities in the FUSE spectra above those predicted by the electron impact model. See text for a detailed discussion.

able at <http://cfa-www.harvard.edu/amp/ampdata/kurucz23/sekur.html>, last modified in 2001), as well as laboratory  $e+N_2$  measurements at 20 and 100 eV [Ajello *et al.*, 1989; James *et al.*, 1990]. Dissociative excitation or ionization from the  $N_2$  ground state is energetically impossible at 20 eV, so a comparison of 20- and 100-eV spectra enables unambiguous identification of atomic and ionic nitrogen transitions when overlap with  $N_2$  transitions is negligible.

## 5. Results and Discussion

[29] In Figures 1 and 2, the 500 K model spectrum is compared with the FUSE observations in regions containing the  $c'_4 \ ^1\Sigma_u^+(0) \sim b' \ ^1\Sigma_u^+(1) - X \ ^1\Sigma_g^+(v_i = 2 - 9)$  emission bands. In Figure 3, the comparable results for  $v_i = 0$  and

1 are presented. Additional atomic and ionic transitions are labeled, as well as  $N_2$  emission bands originating from excited states other than  $b' \ ^1\Sigma_u^+(1)$  and  $c'_4 \ ^1\Sigma_u^+(0)$ . The model spectra have been scaled by a common normalization factor based on a best fit to the FUSE results for  $v_i = 2, 8$  and  $9$ .

### 5.1. Comparison of Observed and Calculated Intensities

[30] Where the  $c'_4 \ ^1\Sigma_u^+(0) \sim b' \ ^1\Sigma_u^+(1) - X \ ^1\Sigma_g^+(2-9)$  bands are relatively free from overlapping features, the calculated relative emission rates clearly agree well with the FUSE observations, particularly for the reference transitions to  $v_i = 2, 8$  and  $9$ . For these three bands, the intensity discrepancy is within  $\pm 4\%$ , even neglecting allowance for a possible overlap with an O III transition at 1184.174 Å. The expected

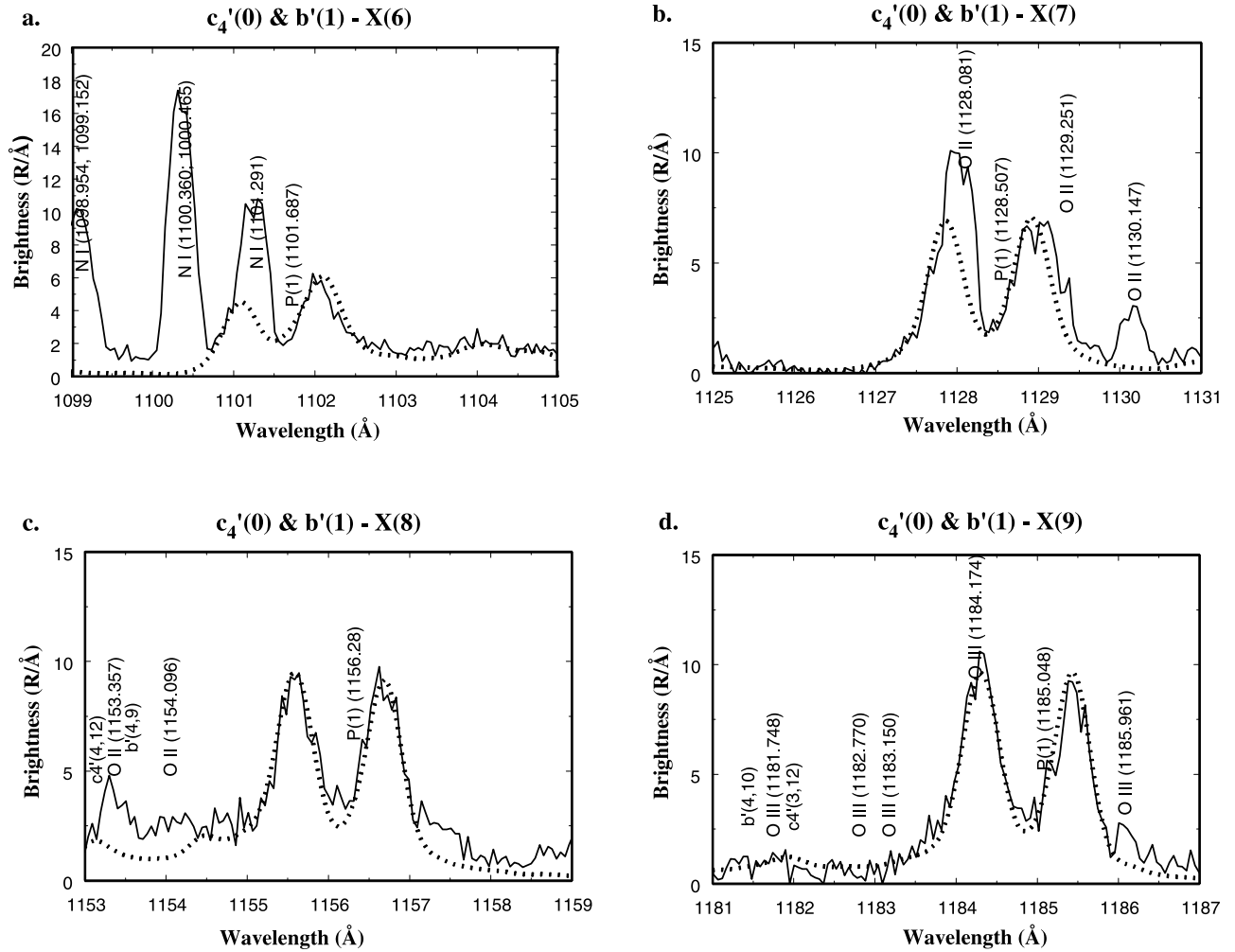


**Figure 2.** Comparison of FUSE observed (solid curves) and model calculated (dotted curves) spectra in the neighborhood of the  $c'_4$   $^1\Sigma_u^+(0) \sim b'$   $^1\Sigma_u^+(1) - X^1\Sigma_g^+(v_i = 6-9)$  emission bands. See Figure 1 caption.

uncertainty in the FUSE spectra encompassing the  $v_i = 8$  and 9 emission bands, covered by the LiF1b detector, is  $\pm 15\%$ .

[31] Intensities for the  $c'_4$   $^1\Sigma_u^+(0) \sim b'$   $^1\Sigma_u^+(1) - X^1\Sigma_g^+(0, 1)$  thermospheric emission bands, known to be attenuated significantly by multiple scattering and resonant, or nearly resonant, absorption, are therefore overestimated by our model which does not include these effects. Further analysis of these bands is performed in sections 5.4 and 5.3.

[32] Figure 1a shows an observed  $c'_4$   $^1\Sigma_u^+(0) \sim b'$   $^1\Sigma_u^+(1) - X^1\Sigma_g^+(2)$  emission band that is a little narrower than in the model spectrum. This is likely to be the result of secondary emission during the multiple scattering of  $c'_4$   $^1\Sigma_u^+(0) - X^1\Sigma_g^+(0)$ , caused by  $J$ -dependent predissociation, aspects that are discussed further in section 5.3.

[33] The  $R$  branch (shorter-wavelength lobe) of the  $c'_4$   $^1\Sigma_u^+(0) \sim b'$   $^1\Sigma_u^+(1) - X^1\Sigma_g^+(3)$  band in Figure 1b is overlapped by a strong H I Lyman- $\beta$  line at 1025.722 Å and the O I  $2s^22p^3(^4S)3d\ ^4D - 2s^22p^4\ ^3P_2$  transition at 1025.762 Å. The  $P$  branch (longer-wavelength) transitions are overlapped by N I  $2s^22p^2(^3P)12d\ ^2D - 2s^22p^3\ ^2D_{5/2}$  and  $2s^22p^2(^3P)12d\ ^2D - 2s^22p^3\ ^2D_{3/2}$  at 1026.69 and 1026.78 Å, respectively, as well as the spin-forbidden  $2s^22p^2(^3P)12d\ ^4P - 2s^22p^3\ ^2D_{5/2}$  and  $2s^22p^2(^3P)12d\ ^4P -$

$2s^22p^3\ ^2D_{3/2}$  lines at 1027.15 and 1027.24 Å [Liu *et al.*, 2008]. According to the electron impact measurements of Liu *et al.* [2008], taken at 100 eV and 300 K, the atomic nitrogen transitions contribute 35–40% of the total intensity between 1026.5 and 1027.7 Å. This contribution is consistent with the model discrepancy seen on the  $P$  branch side of the  $c'_4$   $^1\Sigma_u^+(0) \sim b'$   $^1\Sigma_u^+(1) - X^1\Sigma_g^+(3)$  band in Figure 1b.

[34] In Figure 1c, the calculated emission rate within the  $P$  branch of the  $c'_4$   $^1\Sigma_u^+(0) \sim b'$   $^1\Sigma_u^+(1) - X^1\Sigma_g^+(4)$  band differs by  $\sim 0.8$  R/Å from the FUSE spectrum, a divergence of  $\sim 25\%$ . The  $R$  branch difference is somewhat larger because of the overlapping  $b'$   $^1\Sigma_u^+(4) - X^1\Sigma_g^+(5)$   $N_2$  band. In section 5.2, it is shown that the  $b'$   $^1\Sigma_u^+(4) - X^1\Sigma_g^+(5)$  intensity is enhanced following resonant photoexcitation by the solar H I Lyman- $\epsilon$  line. On the basis of comparative laboratory measurements, the peak labeled N\* in Figure 1c near 1047.5 Å is attributed mainly to N or N\*, with a weak  $b^1\Pi_u(5) - X^1\Sigma_g^+(4)$  contribution.

[35] The  $3p\pi E^1\Pi(0) - X^1\Sigma^+(0)$  emission band of CO, with an origin at 1076.079 Å, overlaps the  $c'_4$   $^1\Sigma_u^+(0) \sim b'$   $^1\Sigma_u^+(1) - X^1\Sigma_g^+(5)$  band of  $N_2$  in Figure 1d. Since the rotational constant of  $E^1\Pi(0)$  is slightly greater than that of  $X^1\Sigma^+(0)$ , most of the spectral intensity is on the blue

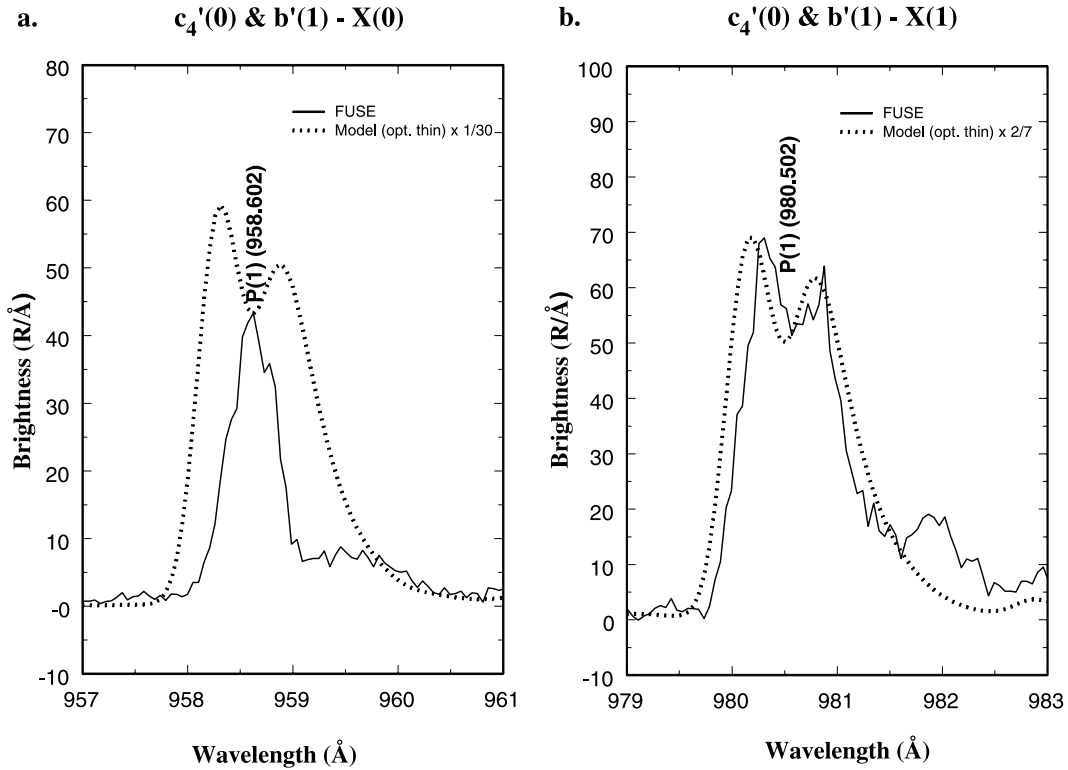


**Figure 3.** Comparison of FUSE observed (solid curves) and optically thin model calculated (dotted curves) spectra near the  $c'_4 \ ^1\Sigma_u^+(0) \sim b' \ ^1\Sigma_u^+(1) - X^1\Sigma_g^+(v_i = 0,1)$  emission bands. (a) The optically thin model spectrum has been scaled down by an additional factor of 30 beyond the common normalization applied to all modeled bands. The FWHMs of the observed and model spectra are  $\sim 0.55$  and  $\sim 1.3$  Å, respectively. Note the nearly complete disappearance of the high- $J$  wings of this band. The peak of the observed spectrum is coincident with the  $P(1)$  transition, where a valley is predicted by the optically thin model. (b) The model spectrum has been reduced by a additional factor of 3.5. The observed band is also narrower than the model prediction. The model-underestimated spectral feature between 982 and 983 Å is primarily due to the  $c_3 \ ^1\Pi_u(0) - X^1\Sigma_g^+(1)$  emission band, with the discrepancy exaggerated by the adopted  $3.5\times$  scaling factor. See section 5.3 for a detailed discussion.

side of the origin [Eidelsberg *et al.*, 1991]. The  $E \ ^1\Pi(0) - X^1\Sigma^+(0)$  band has the second-largest CO oscillator strength, after  $3s\sigma B \ ^1\Sigma^+(0) - X^1\Sigma^+(0)$ , and a predissociation yield of 78.4–88.9% [Cacciani *et al.*, 1998], whereas  $E \ ^1\Pi(1) - X^1\Sigma^+(0)$ , near 1051.714 Å, has a  $<7\%$  relative oscillator strength and a higher predissociation yield of 97.2–98.6%, and is thus too weak to be seen by FUSE. (The  $3s\sigma B \ ^1\Sigma^+(0) - X^1\Sigma^+(0)$  band, at 1087.913 Å, was not observed in a scanned region.)

[36] While the  $P$  branch region of the  $c'_4 \ ^1\Sigma_u^+(0) \sim b' \ ^1\Sigma_u^+(1) - X^1\Sigma_g^+(6)$  band in Figure 2a is relatively unobscured, the  $R$  branch is overlapped by one of three strong atomic nitrogen lines. The first of these, at 1099.1 Å, arises from two  $2s^22p^2(^3P)4d \ ^2P_{3/2} - 2s^22p^3 \ ^2D_J$  fine-structure transitions ( $J = 5/2$  and  $3/2$ ) and four  $2s^22p^2(^3P)4d \ ^4F - 2s^22p^3 \ ^2D$  spin-forbidden transitions [see also Liu *et al.*, 2008]. The feature at 1100.4 Å consists of the  $2s^22p^2(^3P)5s \ ^2P_{3/2} - 2s^22p^3 \ ^2D_{5/2}$  (1100.360 Å) and  $2s^22p^2(^3P)5s \ ^2P_{3/2} - 2s^22p^3 \ ^2D_{3/2}$  (1100.465 Å) transitions, while that at 1101.3 Å arises from the  $2s^22p^2(^3P)5s \ ^2P_{1/2} - 2s^22p^3 \ ^2D_{3/2}$  transition (1100.291 Å). If the population ratio  $5s \ ^2P_{3/2}:5s \ ^2P_{1/2}$  is equal to the degeneracy ratio 2:1, the observed intensity of the 1101.291 Å feature will be half

that of the 1100.360 and 1100.465 Å transitions [Ralchenko *et al.*, 2007]. The spin-forbidden  $2s^22p^2(^3P)5s \ ^4P_{5/2} - 2s^22p^3 \ ^2D_{5/2}$  (1102.509 Å) and  $2s^22p^2(^3P)5s \ ^4P_{5/2} - 2s^22p^3 \ ^2D_{3/2}$  (1102.615 Å) atomic nitrogen transitions are possible weak emitters contributing to the  $P$  branch region of the  $c'_4 \ ^1\Sigma_u^+(0) \sim b' \ ^1\Sigma_u^+(1) - X^1\Sigma_g^+(6)$  band, but there is no real indication of their presence in Figure 2a. In fact, both laboratory measurements [Liu *et al.*, 2008] and calculations (P. L. Smith *et al.*, 1995 atomic line data (R. L. Kurucz and B. Bell), Kurucz CD-ROM 23, Smithsonian Astrophysics Observatory, Cambridge, Massachusetts, available at <http://cfa-www.harvard.edu/amp/ampdata/kurucz23/sekur.html>, last modified in 2001) have shown that these two lines are weaker than the  $2s^22p^2(^3P)5s \ ^4P_{1/2} - 2s^22p^3 \ ^2D_{3/2}$  transition expected at 1104.008 Å. While the experimental trace in Figure 2a shows a small bump near 1104 Å, this is consistent with the  $c_3 \ ^1\Pi_u(0) - X^1\Sigma_g^+(6)$  band transition in the model spectrum. Thus, the contribution of N I emission to the  $P$  branch region is determined to be negligible. Under the above assumptions, the observed integrated  $N_2$  surface brightness, between 1100 and 1103.1 Å, is inferred to be 7.3 R,  $\sim 15\%$  lower than predicted by the model (8.6 R).

[37] Three O II lines in Figure 2b severely overlap the  $c'_4$   $^1\Sigma_u^+(0) \sim b'^1\Sigma_u^+(1) - X^1\Sigma_g^+(7)$  band of  $N_2$ . Features at 1128.081, 1129.251 and 1130.147 Å arise from the  $2s^2 2p^2(^3P)3p^4P^o_{5/2} - 2s2p^4^4P_{5/2}$ ,  $2s^2 2p^2(^3P)3p^4P^o_{3/2} - 2s2p^4^4P_{5/2}$ , and  $2s^2 2p^2(^4P)3p^4P^o_{5/2} - 2s2p^4^4P_{3/2}$  transitions of O II, respectively. On the basis of the transition probabilities listed by *Ralchenko et al.* [2007], the O II contribution to the peak at 1128 Å should be  $\sim 2.5\times$  the intensity of the 1130.147 Å line. The FUSE emission rate for the 1128 Å peak should then correspond to the modeled  $N_2$  emission rate plus  $2.5\times$  the FUSE emission strength of the O II 1130.147 Å line. However, the integrated strength of the observed 1128 Å feature is only  $\sim 87\%$  of this sum, implying, under the above assumption, that the modeled  $N_2$   $R$  branch emission rate is a  $\sim 20\%$  overestimate. The observed  $P$  branch region includes a contribution from the O II  $J = 3/2$  fine-structure component at 1129.251 Å. If, according to the relative level degeneracies, the population of the  $J = 3/2$  level is  $2/3\times$  that of  $J = 5/2$ , then a comparison between the observed and model spectra in Figure 2b implies that the model intensity for the  $N_2$   $P$  branch is  $\sim 10\%$  too high. These  $R$  and  $P$  branch discrepancies are of the same order as the 15% observational uncertainty.

[38] In the calibration regions of Figures 2c and 2d, respectively, there is very good agreement between the shapes of the observed and calculated  $c'_4$   $^1\Sigma_u^+(0) \sim b'^1\Sigma_u^+(1) - X^1\Sigma_g^+(8,9)$  emission spectra. However, it should be noted that there is the possibility of weak contamination of the  $R$  branch of the latter band by the O III  $2s2p^2(^4P)4d^5P - 2s2p^2(^4P)2p^5D^o$  transition at 1184.174 Å.

## 5.2. Resonant Solar Photoexcitation of $N_2$

[39] Figures 1 and 2 demonstrate consistent model underestimation of emission from  $N_2$   $b'^1\Sigma_u^+(4)$  and  $b'^1\Sigma_u^+(7)$ , with a discrepancy more than 4 times the expected maximum combined error of model and observation. The error includes observation uncertainty equivalent to  $\leq 35\%$  of the corresponding e +  $N_2$  model intensities, 10% model uncertainty from oscillator strength, 12% model uncertainty from excitation functions and photoelectron energy, and an assumed  $\leq 40\%$  error in predissociation yields averaged over  $J_j$  at 500K. These estimated components result in an overall  $\leq 55\%$  probable combined error and 97% maximum combined error, both of which are relative to corresponding calculated e +  $N_2$  emission intensities as normalized in Figures 1 and 2. The unmodeled intensity detected from these levels is likely to arise from the omission of excitation channels other than electron scattering of  $X^1\Sigma_g^+$ .

[40] Resonant excitation by the  $n = 6$  and 12 lines of the solar H I Lyman series is most likely responsible for the additional excitation of some rotational levels of  $b'^1\Sigma_u^+(4)$  and  $b'^1\Sigma_u^+(7)$ . A previous FUSE observation employing the MDRS aperture, by *Feldman et al.* [2001], found extensive and prominent emission from Lyman series transitions with  $n$  as high as 28. The variation of spectral intensity with  $n$  was found to be highly irregular, with observed intensities of the Lyman- $\gamma$  and Lyman- $\epsilon$  lines noticeably weak. The  $b'^1\Sigma_u^+(7) - X^1\Sigma_g^+(0)$   $P(5)$ ,  $P(6)$ ,  $R(9)$ , and  $R(10)$  rotational transitions at 918.109, 918.196, 918.067, and 918.141 Å may be excited by the H I Lyman ( $n = 12 \rightarrow n = 1$ ) line at 918.129 Å, while the  $b'^1\Sigma_u^+(4) - X^1\Sigma_g^+(0)$   $P(2)$ ,  $P(3)$ ,  $R(6)$ ,

and  $R(7)$  lines at 937.759, 937.821, 937.783 and 937.844 Å may be excited by Lyman- $\epsilon$  ( $n = 6 \rightarrow n = 1$ ) at 937.803 Å. At a temperature of 500K, all of these rotational transitions have significant lower state populations. The excitation and dissociation of  $N_2$  by the solar Lyman series have been examined in detail by *Shemansky et al.* (manuscript in preparation, 2009).

[41] Other solar lines may also play a role. For example, the  $b'^1\Sigma_u^+(4) - X^1\Sigma_g^+(0)$   $P(10)$  rotational transition may be directly excited by the solar O I line  $2s^2 2p^3(^4S^o)6d^3D^o_1 - 2s^2 2p^4^3P_0$  (938.625 Å), as may  $P(5)$ ,  $P(6)$ , and  $R(11)$ , by O I  $2s^2 2p^3(^4S^o)6d^3D^o - 2s^2 2p^4^3P_1$  (938.020 Å), as well as  $P(2-4)$  and  $R(6-8)$ , by O I  $2s^2 2p^3(^4S^o)7s^3S^o - 2s^2 2p^4^3P_1$  (937.843 Å). The 937.843, 938.020 Å, and H Lyman- $\epsilon$  solar features are not resolved in the current observations, but the line at 938.020 Å has been observed by *Feldman et al.* [2001], as was the 938.625 Å line, with significant intensity.

[42] The  $b'^1\Sigma_u^+(4) - X^1\Sigma_g^+(1)$  oscillator strength is fairly significant, suggesting that a further possible  $b'^1\Sigma_u^+(4)$  photoexcitation mechanism is reabsorption of radiation from the nearly coincident  $c'_4$   $^1\Sigma_u^+(0) - X^1\Sigma_g^+(0)$  emission band. The  $c'_4$   $^1\Sigma_u^+(0) - X^1\Sigma_g^+(0)$  optically thin brightness, inferred in section 5.4, is  $\sim 100\times$  greater than the combined brightness of the H I and O I transitions considered above. Furthermore, the oscillator strength of  $b'^1\Sigma_u^+(4) - X^1\Sigma_g^+(1)$  is  $9\times$  larger than that of  $b'^1\Sigma_u^+(4) - X^1\Sigma_g^+(0)$  and, assuming local thermodynamic equilibrium (LTE) at 500 K, ground state  $N_2$  will consist of  $\sim 0.12\%$   $v_i = 1$ . This would be sufficient to make the pumping of  $b'^1\Sigma_u^+(4)$  from  $X^1\Sigma_g^+(1)$  by  $c'_4$   $^1\Sigma_u^+(0) - X^1\Sigma_g^+(0)$  emission as important as excitation from  $X^1\Sigma_g^+(0)$  by the solar Lyman- $\epsilon$  line. A non-LTE vibrationally excited ground state, which would increase the importance of the former process, may result from excited state emission to  $v_i > 0$  levels, or by low-energy ( $< 5$  eV) electron impact, a process known to have a large vibrational cross section in  $N_2$  [*Schultz, 1964; Boness and Schulz, 1973; Allan, 1985; Vicic et al., 1996; Dube and Herzenberg, 1979; Morgan, 1986; Sun et al., 1995; Grimm-Bosbach et al., 1996*]. Furthermore, any nonthermal population of  $X^1\Sigma_g^+(1)$  will have a long spontaneous emission lifetime because  $N_2$  possesses no permanent dipole moment and only a small quadrupole transition moment in the  $X^1\Sigma_g^+$  state. The peak electron impact cross section for the  $c'_4$   $^1\Sigma_u^+(0) - X^1\Sigma_g^+(0)$  excitation near 75 eV, the largest of any  $N_2$  singlet ungerade vibrational transition, is  $\sim 7.7 \times 10^{-18}$   $\text{cm}^2$  [*Liu et al., 2005b*]. In contrast, the  $X^1\Sigma_g^+(0) \rightarrow X^1\Sigma_g^+(1)$  excitation cross section at 2.3 eV is  $\sim 5.6 \times 10^{-16}$   $\text{cm}^2$  [*Robertson et al., 1997*]. Clearly, a small percentage of photoelectrons with energy between 1.5 and 5 eV can make vibrational excitation (and deactivation) a very important process.

[43] Finally, we note that resonant excitation of the  $b^1\Pi_u(3)$ ,  $b^1\Pi_u(6)$ ,  $b'^1\Sigma_u^+(6)$ , and, possibly,  $b^1\Pi_u(10)$  levels of  $N_2$  by solar radiation has also been observed. Further details are given by *Shemansky et al.* (manuscript in preparation, 2009).

## 5.3. Multiple Scattering, Predissociation, and the $c'_4$ $^1\Sigma_u^+(0) \sim b'^1\Sigma_u^+(1) - X^1\Sigma_g^+$ Band Shape

[44] A clear physical picture of the  $c'_4$   $^1\Sigma_u^+(0)$  predissociation mechanism is necessary in order to understand the radiation loss and band shape distortion demonstrated by the  $c'_4$   $^1\Sigma_u^+(0) \sim b'^1\Sigma_u^+(1) - X^1\Sigma_g^+(0)$  emission band. In the

coupled channels picture, predissociation is caused by strong rotational coupling between the diabatic  $c'_4$   $^1\Sigma_u^+$  and  $c_3$   $\Pi_u^e$  states, both of which are members of a  $3p$  Rydberg complex [Lefebvre-Brion and Field, 2004]. This coupling provides  $c'_4$   $^1\Sigma_u^+(0)$  with its primary  $J_j$ -dependent predissociation effect, induced by  $^1\Pi_u^e$  levels, which in turn, are predissociated by the  $C$  and  $C'$   $^3\Pi_u$  states via spin-orbit coupling [Lewis *et al.*, 2005a, 2005b; Haverd *et al.*, 2005]. Because the  $^1\Sigma_u^+ \sim ^1\Pi_u^e$  coupling matrix elements are proportional to  $[J(J_j + 1)]^{1/2}$ , the predissociation of  $c'_4$   $^1\Sigma_u^+(0)$  is slow for the very low  $J_j$  levels, but increases rapidly with  $J_j$ . In particular, the  $J_j = 0$  level is uncoupled from the  $^1\Pi_u^e$  states and can, therefore, be considered free from predissociation due to this primary mechanism.

[45] In Figure 3a, the spectrum observed by FUSE in the region of the  $c'_4$   $^1\Sigma_u^+(0) \sim b'^1\Sigma_u^+(1) - X^1\Sigma_g^+(0)$  emission band is shown. For comparison, the optically thin model spectrum, scaled down by a factor of 30, is also indicated. Two important features are apparent. First, the width of the observed band spectrum ( $\sim 0.55$  Å FWHM) is significantly smaller than the modeled width ( $\sim 1.3$  Å FWHM). Second, the peak of the observed spectrum coincides with the  $P(1)$  rotational transition at 958.6 Å, where a trough is seen in the optically thin model and laboratory spectra [Liu *et al.*, 2008, Figure 2a].

[46] The drastic decrease of observed FUSE brightness and band width is consistent with a multicycle of emission and resonant absorption, with radiation lost both through predissociation and emission to  $X^1\Sigma_g^+(v_i > 0)$ . The  $c'_4$   $^1\Sigma_u^+(0) - X^1\Sigma_g^+(0)$   $P(1)$  line ( $J_j = 0$ ) has an emission branching ratio of 0.843, the largest of any rotational transition within this band, and is therefore the most resistant to radiation loss. Nevertheless, there is a loss of 15.7% of  $P(1)$  intensity during every cycle of reemission. A simple estimate based on this number suggests that a factor of 30 decrease in the observed  $P(1)$  emission rate corresponds to, on average,  $\sim 20$  emission absorption cycles before detection. The radiation lost from higher- $J_j$  transitions progressively increases because of increasing predissociation losses. For example, the  $J_j = 7$  level decays to  $X^1\Sigma_g^+(0)$  with an emission branching ratio of 0.716. Then, 20 cycles of emission and resonant absorption would decrease the FUSE intensities of the resultant  $P(8)$  and  $R(6)$  lines by a factor of  $\sim 800$ . The losses for the higher- $J_j$  levels clearly are even more drastic, which explains the negligible emission rate on the blue side of  $R(6)$  ( $< 958.34$  Å) and the red side of  $P(8)$  ( $> 959.89$  Å) in Figure 3a. This explanation is in agreement with the peak observed emission rate coinciding with the  $P(1)$  transition and the conclusions of Bishop *et al.* [2007], who found that consideration of only transitions involving  $J_j \leq 7$  was sufficient to approximate the shape of the (0,0) band.

[47] For each  $c'_4$   $^1\Sigma_u^+(0) - X^1\Sigma_g^+(0)$  resonant absorption and emission cycle, a fraction of the emission is transferred to  $c'_4$   $^1\Sigma_u^+(0) - X^1\Sigma_g^+(v_i > 0)$  transitions. These alternative emission pathways compete with  $c'_4$   $^1\Sigma_u^+(0)$  predissociation and so will also preferentially augment the low  $J_j$  lines of  $v_i > 0$  emission, resulting in a narrowing of the profiles of the corresponding bands. This narrowing phenomenon is apparent in Figure 3b, which compares the FUSE and optically thin model spectra for the  $c'_4$   $^1\Sigma_u^+(0) - X^1\Sigma_g^+(1)$  band. The observed emission rate of this band is  $\sim 3.5 \times$  weaker than predicted by the model (which has been scaled

down in Figure 3b). This reduction in intensity is due to resonant absorption by the nearly coincident transition  $b'^1\Pi_u(2) - X^1\Sigma_g^+(0)$ , where the  $b'^1\Pi_u(2)$  level is strongly predissociated [Stevens *et al.*, 1994]. Whether resonant absorption by  $X^1\Sigma_g^+(1)$  plays any significant role will likely be dependent on the extent of non-LTE effects. Some spectral narrowing is also observed in Figure 1a, in the region of the  $c'_4$   $^1\Sigma_u^+(0) - X^1\Sigma_g^+(2)$   $P$  branch, on the long-wavelength side. The presumed similar narrowing for the  $R$  branch is obscured because of overlapping solar-enhanced  $b'^1\Sigma_u^+(7) - X^1\Sigma_g^+(4)$  emission, as discussed in section 5.2. Indeed, the small peak at 1003.13 Å in the observed spectrum, if real, could be attributed to the  $P(12)$  transition of  $b'^1\Sigma_u^+(7) - X^1\Sigma_g^+(4)$ . Since the  $c'_4$   $^1\Sigma_u^+(0) \sim b'^1\Sigma_u^+(1) - X^1\Sigma_g^+(2)$   $^1\Sigma_g^+(2)$  band is used as part of our intensity normalization procedure (see section 5.1), it is not possible to determine whether any intensity anomalies are present in this band.

[48] Neither intensity nor band shape anomalies are apparent in any of the spectra of Figure 2. First, the effects of multiple scattering and predissociation on the emission intensities to  $X^1\Sigma_g^+(v_i > 2)$  levels are negligible, because the ground state populations with  $v_i > 2$  are too small to support radiation trapping. Second, since the valence  $b'^1\Sigma_u^+(1)$  level has a significantly greater Franck-Condon overlap with the  $v_i > 2$  ground state levels than does the Rydberg  $c'_4$   $^1\Sigma_u^+(0)$  level, the combined emission from  $c'_4$   $^1\Sigma_u^+(0)$  and  $b'^1\Sigma_u^+(1)$  to those levels contains an increasing  $b'^1\Sigma_u^+(1)$  component [Liu *et al.*, 2008]. Therefore, since the predissociation yield of the  $b'^1\Sigma_u^+(1)$  level is much less  $J_j$ -dependent than that of the  $c'_4$   $^1\Sigma_u^+(0)$  level, there is a lower susceptibility to  $c'_4$   $^1\Sigma_u^+(0) \sim b'^1\Sigma_u^+(1) - X^1\Sigma_g^+(v_i > 2)$  band shape distortion following any resonant absorption cycle.

#### 5.4. Integrated Excitation and Emission Rates for the $c'_4$ $^1\Sigma_u^+(0)$ and $b'^1\Sigma_u^+(1)$ Levels

[49] In Table 1, the observed and calculated surface emission rates for the  $c'_4$   $^1\Sigma_u^+(0) \sim b'^1\Sigma_u^+(1) - X^1\Sigma_g^+(v_i)$  combined transitions are compared, with the calculated individual contributions from  $c'_4$   $^1\Sigma_u^+(0)$  and  $b'^1\Sigma_u^+(1)$  also listed. The model calculations refer to an optically thin medium at 500 K, the latter specified since the relative  $c'_4$   $^1\Sigma_u^+(0)$  and  $b'^1\Sigma_u^+(1)$  emission rates depend slightly on the temperature. The last column in Table 1 lists integrated FUSE emission rates, after the contributions from atomic and ionic transitions, and  $N_2$  emission from levels other than  $c'_4$   $^1\Sigma_u^+(0)$  and  $b'^1\Sigma_u^+(1)$ , have been removed, as described in section 5.1. Reliable FUSE integrated emission strengths for transitions terminating on the  $v_i = 3, 4,$  and  $5$  ground state levels cannot be obtained because of heavy overlapping in the corresponding experimental spectra. Furthermore, the serious distortion of the  $c'_4$   $^1\Sigma_u^+(0) \sim b'^1\Sigma_u^+(1) - X^1\Sigma_g^+(0)$  band shape, and consequent uncertainty regarding the role of overlapping features, prevents its brightness from being estimated to a high degree of accuracy.

[50] Apart from the transitions to the  $v_i = 0$  and  $1$  levels, discussed in detail in section 5.3, the calculated and observed band brightnesses in Table 1 agree to within 15%. The physically based model employed here enables a realistic extrapolation to be made by employing the unattenuated observed emission to  $v_i \geq 2$  and the modeled relative band intensities. This permits the inference of an optically thin brightness of 2115 R for emission to  $v_i = 0$ , and 315 R to

**Table 1.** Brightness of the c'<sub>4</sub><sup>1</sup>Σ<sub>u</sub><sup>+</sup>(0)– and b'<sup>1</sup>Σ<sub>u</sub><sup>+</sup>(1) – X<sup>1</sup>Σ<sub>g</sub><sup>+</sup>(v<sub>i</sub>) Bands (R)

v <sub>i</sub>	Model <sup>a</sup> c' <sub>4</sub> <sup>1</sup> Σ <sub>u</sub> <sup>+</sup> (0) – X <sup>1</sup> Σ <sub>g</sub> <sup>+</sup>	Model <sup>a</sup> b' <sup>1</sup> Σ <sub>u</sub> <sup>+</sup> (1) – X <sup>1</sup> Σ <sub>g</sub> <sup>+</sup>	Model <sup>a</sup> Sum	FUSE Observed <sup>b</sup>	Bishop et al. [2007] <sup>c</sup> c' <sub>4</sub> <sup>1</sup> Σ <sub>u</sub> <sup>+</sup> (0) – X <sup>1</sup> Σ <sub>g</sub> <sup>+</sup>
0	2101.6	13.7	2115.4	24 ± 7 <sup>d</sup>	21 ± 7(20 ± 7)
1	312.4	2.12	314.6	79.4 ± 8 <sub>9</sub>	55 ± 18(53 ± 17)
2	35.2	0.40	35.6	35.3 ± 3.6	31 ± 4(29 ± 4)
3	6.00	0.39	6.39		
4	2.55	0.80	3.36		
5	1.98	1.65	3.63		
6	2.80	2.93	5.73	5.2	6 ± 1(6 ± 1)
7	4.12	4.44	8.56	7.3	6 ± 2(5.5 ± 1.8)
8	5.00	5.80	10.8	11.1	13 ± 4(11.2 ± 3.4)
9	5.31	6.50	11.8	11.6	15 ± 4(10.5 ± 2.8)
10	5.00	6.20	11.2		
11	4.03	4.92	8.95		
12	2.53	3.10	5.63		
13	1.14	1.40	2.53		
14	0.290	0.328	0.619		
15	0.021	0.002	0.023		
16	0.107	0.111	0.218		
17	0.186	0.216	0.403		
18	0.099	0.128	0.227		
19	0.008	0.011	0.019		
20	0.020	0.018	0.037		
>20	≤0.4	≤0.4	≤0.8		
Σ(v <sub>i</sub> ≥ 2)	76.8	39.7	116.6		
Σ(v <sub>i</sub> ≥ 0)	2491	55.6	2547 <sup>e</sup>		

<sup>a</sup>Absolute optically thin model brightness inferred by using a normalization constant averaged over the emission bands terminating on v<sub>i</sub> = 2, 8, and 9 (see text), and an N<sub>2</sub> temperature of 500 K.

<sup>b</sup>Estimated from FUSE spectrum after removing the contributions from atomic, ionic, and other overlapping N<sub>2</sub> emissions.

<sup>c</sup>c'<sub>4</sub><sup>1</sup>Σ<sub>u</sub><sup>+</sup>(0) – X<sup>1</sup>Σ<sub>g</sub><sup>+</sup>(v<sub>i</sub>) emission rates reported by Bishop et al. [2007]. Numbers in parentheses are obtained after adjusting for the difference in calibration. Specifically, the rates to v<sub>i</sub> = 7, 8, and 9 have been reduced by 8%, 14%, and 30%, respectively, and rates to the other v<sub>i</sub> levels have been reduced by 5%.

<sup>d</sup>Because of severe distortion in shape, the brightness of this band cannot be partitioned accurately between c'<sub>4</sub><sup>1</sup>Σ<sub>u</sub><sup>+</sup>(0) ~ b'<sup>1</sup>Σ<sub>u</sub><sup>+</sup>(1) – X<sup>1</sup>Σ<sub>g</sub><sup>+</sup>(0) emission and any overlapping features.

<sup>e</sup>If the FUSE-measured brightnesses of 24 R is adopted for emission to v<sub>i</sub> = 0, the total modeled brightness of emission to all ground state levels is ~220 R, only 8.6% of the model-predicted optically thin brightness.

v<sub>i</sub> = 1. Comparing these values with the direct FUSE measurements, the radiation lost during multiple scattering is found to be 99% for emission to v<sub>i</sub> = 0 and 75% to v<sub>i</sub> = 1. Since resonant self-absorption, not included in the model, leads partially to secondary radiation escaping via transitions to v<sub>i</sub> > 0, the extrapolated brightnesses may be overestimated.

[51] Table 1 includes results reported by Bishop et al. [2007], which differ significantly from the present results in several instances. The differences are caused by a combination of calibration and spectral content. The last column of Table 1 lists the original value of the c'<sub>4</sub><sup>1</sup>Σ<sub>u</sub><sup>+</sup>(0) – X<sup>1</sup>Σ<sub>g</sub><sup>+</sup>(v<sub>i</sub>) bands obtained by Bishop et al. and the value (in parentheses) after adjustment of the difference in calibration. Specifically, the original values for the v<sub>i</sub> = 7, 8 and 9 bands have been reduced by 8%, 14%, and 30%, respectively. For the v<sub>i</sub> < 7 levels, the original Bishop et al. values have been reduced by 5%. Given that Bishop et al. utilized a Hönl-London-factor-based photoabsorption model that excludes the contribution from the b'<sup>1</sup>Σ<sub>u</sub><sup>+</sup>(1) level, it is necessary to compare their adjusted values to the emission rates in the fourth (v<sub>i</sub> > 1) and fifth columns. For transitions terminating in v<sub>i</sub> = 1 and 2, the adjusted Bishop et al. and the present (fifth column) values are outside either error range. Bishop et al. [2007] inserted the N I 2s2p<sup>4</sup> 2D – 2s<sup>2</sup>2p<sup>3</sup> 2D<sup>o</sup> transitions at 980.632 and 980.706 Å to improve their fit in the P branch side of the (0, 1) band and attributed 4 R to the N I emission. However, high-resolution electron impact experimental work by Liu et al. [2008] failed to detect these transitions. The present work shows in Figure 3b that the CSE calculation reproduces the

observed P/R branch relative intensity, and the introduction of N I lines is not necessary. If the 4 R allocated to the N I emission is added back to N<sub>2</sub> (0, 1) band, the difference between two values is still outside of either error range. For the emissions to the v<sub>i</sub> = 6–9 levels, Table 1 shows that the contribution of the b'<sup>1</sup>Σ<sub>u</sub><sup>+</sup>(1) – X<sup>1</sup>Σ<sub>g</sub><sup>+</sup> is more important than the c'<sub>4</sub><sup>1</sup>Σ<sub>u</sub><sup>+</sup>(0) – X<sup>1</sup>Σ<sub>g</sub><sup>+</sup> transition. For these bands, the treatment by Bishop et al. [2007] significantly underestimated the relative intensity of the R branches. In the case of v<sub>i</sub> = 8 and 9, Bishop et al. [2007] underestimated the intensities on the R branch side by approximately 30–40%, which translates into 15–20% reduction in their c'<sub>4</sub><sup>1</sup>Σ<sub>u</sub><sup>+</sup>(0) emission rates. Additionally, Bishop et al. did not consider contributions of the overlapping N<sub>2</sub> emission from levels other than c'<sub>4</sub><sup>1</sup>Σ<sub>u</sub><sup>+</sup>(0) and b'<sup>1</sup>Σ<sub>u</sub><sup>+</sup>(1) and attributed the all observed nearby N<sub>2</sub> intensity to the c'<sub>4</sub><sup>1</sup>Σ<sub>u</sub><sup>+</sup>(0) emission. As noted in section 4, the present work considers all emissions from b'<sup>1</sup>Σ<sub>u</sub><sup>+</sup>(v<sub>j</sub> = 0–14), b<sup>1</sup>Π<sub>u</sub>(v<sub>j</sub> = 0–14), c'<sub>4</sub><sup>1</sup>Σ<sub>u</sub><sup>+</sup>(v<sub>j</sub> = 0–4), and c<sub>3</sub><sup>1</sup>Π<sub>u</sub>(v<sub>j</sub> = 0–1), for rotational levels up to J<sub>j</sub> = 30. For the (0, 7), (0, 8) and (0, 9) bands, the present analysis shows that N<sub>2</sub> emission from non-c'<sub>4</sub><sup>1</sup>Σ<sub>u</sub><sup>+</sup>(0) and non-b'<sup>1</sup>Σ<sub>u</sub><sup>+</sup>(1) levels contributes about 10%, 17% and 13% of the observed N<sub>2</sub> intensities in the 1129.872–1130.496, 1154.885–1157.172 and 1183.328–1185.773 Å regions, respectively. Thus, the Bishop et al. underestimation of the intensity on the R branch side is roughly offset by the attribution of the non-c'<sub>4</sub><sup>1</sup>Σ<sub>u</sub><sup>+</sup>(0) and non-b'<sup>1</sup>Σ<sub>u</sub><sup>+</sup>(1) emission to the c'<sub>4</sub><sup>1</sup>Σ<sub>u</sub><sup>+</sup>(0) and b'<sup>1</sup>Σ<sub>u</sub><sup>+</sup>(1) levels.

[52] On the basis of our CSE calculations, the rotationally averaged predissociation yields following electron impact excitation of  $c'_4$   $^1\Sigma_u^+(0)$  and  $b' ^1\Sigma_u^+(1)$  at 500 K are  $\sim 25\%$  and  $\sim 53\%$ , respectively. The model total, column-integrated, optically thin emission rates to all ground state levels considered are  $2.49 \times 10^9$  and  $5.56 \times 10^7$   $\text{cm}^{-2} \text{s}^{-1}$ , respectively. Using these data in equation (1), an estimate is obtained of the electron impact excitation rate into  $c'_4$   $^1\Sigma_u^+(0)$ , namely  $3.3 \times 10^9$   $\text{cm}^{-2} \text{s}^{-1}$ . Similarly, the excitation into  $b' ^1\Sigma_u^+(1)$  is modeled to occur at a rate of  $1.2 \times 10^8$   $\text{cm}^{-2} \text{s}^{-1}$ . These rates are constrained experimentally by the normalization of the model spectra to the FUSE observations.

[53] The combined column-integrated excitation rate to the  $c'_4$   $^1\Sigma_u^+(0)$  and  $b' ^1\Sigma_u^+(1)$ ,  $3.4 \times 10^9$   $\text{cm}^{-2} \text{s}^{-1}$ , is significantly larger than the value  $1.4 \times 10^9$   $\text{cm}^{-2} \text{s}^{-1}$  obtained by Bishop *et al.* [2007]. The difference is largely caused by the difference in emission branching ratios given that the excitation rate is inferred from the observed brightness. A small error in branching ratio can lead to a very significant difference in the inferred  $c'_4$   $^1\Sigma_u^+(0)$  excitation rate because of the small branching ratios of the  $c'_4$   $^1\Sigma_u^+(0) - X^1\Sigma_g^+(v_i \geq 2)$  transitions. Bishop *et al.* [2007] obtained their branching ratio from emission cross sections of Ajello *et al.* [1989], in which measurement was limited to  $v_i = 0-5$ . The  $b' ^1\Sigma_u^+(1)$  and  $c'_4$   $^1\Sigma_u^+(0)$  emissions up to  $v_i \leq 13$  are clearly observable in the laboratory measurement and relative intensities are accurately reproduced by the CSE calculation (see columns 2, 3, and 4 of Table 1). Thus, the limited summation of emission cross sections ( $v_i = 0-5$ ) by Bishop *et al.* [2007] excludes a significant part of the sequence. Moreover, accurate evaluation of emission branching ratios also requires proper treatment of overlapped emissions. In the work by Ajello *et al.* [1989], the contribution of the  $b' ^1\Sigma_u^+(1)$  emission to the observed intensities was attributed to the  $c'_4$   $^1\Sigma_u^+(0)$ . While other  $N_2$  transitions that overlap with the  $c'_4$   $^1\Sigma_u^+(0) - X^1\Sigma_g^+$  transitions were tabulated, the relative contribution of these overlapped transitions could not be separated in that work. The difference in branching ratios is also partly attributed to the different treatment of predissociation. Bishop *et al.* [2007] utilized a constant predissociation yield for  $J = 0-5$  levels and 100% for  $J \geq 6$  levels, while the present work used CSE calculated  $J$ -dependent predissociation rates and considered excitation to  $J_j = 0-30$  levels. The emission branching ratios used by Bishop *et al.* for the (0,0) band in their Figure 1a are inconsistent with those for the (0,  $v_i > 0$ ) bands in their Figures 1b, 1c, 2, and 3. Since the present work utilized the intrinsically more accurate emission branching ratios, the present excitation rate is superior to the Bishop *et al.* [2007] result.

## 6. Summary and Conclusions

[54] Terrestrial thermospheric  $N_2$   $c'_4$   $^1\Sigma_u^+(0) \sim b' ^1\Sigma_u^+(1) - X^1\Sigma_g^+(2-9)$  dayglow emission observed in FUSE measurements has been modeled quantitatively, with the assumption of photoelectron impact as the principal molecular excitation mechanism. Very good agreement has been achieved between the model and observations for the  $v_i = 2$ , and 6-9 levels. Reliable estimates of the emission rates to the  $v_i = 3-5$  levels are also provided. In addition, a number of resonant excitations by solar radiation have been identified.

The  $c'_4$   $^1\Sigma_u^+(0) \sim b' ^1\Sigma_u^+(1) - X^1\Sigma_g^+$  combined emission rates and an estimate of the excitation rates have been determined. The significantly reduced observed emission rate of  $c'_4$   $^1\Sigma_u^+(0) \sim b' ^1\Sigma_u^+(1) - X^1\Sigma_g^+(0)$  and distortion of the  $c'_4$   $^1\Sigma_u^+(0) \sim b' ^1\Sigma_u^+(1) - X^1\Sigma_g^+(0-2)$  band shapes have also been explained qualitatively in terms of multiple scattering, predissociation, and radiative escape.

[55] **Acknowledgments.** This work was partially supported by the Cassini UVIS contract with the University of Colorado and NASA-NNG06GH76G issued to SET through the Planetary Atmospheres Program. This work was also partially supported by Australian Research Council Discovery Program grants DP0558962 and DP0773050. We thank Van Dixon and Mary Romelfanger for their assistance with the data reprocessing. This work is based on data obtained by the NASA-CNES-CSA FUSE mission operated by the Johns Hopkins University under NASA contract NASS-32985.

## References

- Abgrall, H., and E. Roueff (2006), Theoretical calculations of excited rovibrational levels of HD. Term values and transition probabilities of VUV electronic bands, *Astron. Astrophys.*, *445*, 361-372, doi:10.1051/0004-6361:20053694.
- Ajello, J. M., G. K. James, B. O. Franklin, and D. E. Shemansky (1989), Medium-resolution studies of extreme ultraviolet emission from  $N_2$  by electron impact: Vibrational perturbations and cross sections of the  $c'_4$   $^1\Sigma_u^+$  and  $b' ^1\Sigma_u^+$  states, *Phys. Rev. A*, *40*, 3524-3555, doi:10.1103/PhysRevA.40.3524.
- Ajello, J. M., M. H. Stevens, I. Stewart, K. Larsen, L. Esposito, J. Colwell, W. McClintock, G. Holsclaw, J. Gustin, and W. Pryor (2007), Titan airglow spectra from Cassini Ultraviolet Spectrograph (UVIS): EUV analysis, *Geophys. Res. Lett.*, *34*, L24204, doi:10.1029/2007GL031555.
- Allan, M. (1985), Excitation of vibrational levels up to  $v = 17$  in  $N_2$  by electron impact in the 0-5 eV region, *J. Phys. B*, *18*, 4511-4517, doi:10.1088/0022-3700/18/22/018.
- Berkowitz, J. (2002), *Atomic and Molecular Photoabsorption: Absolute Total Cross Sections*, pp. 140-147, Academic, San Diego, Calif.
- Bishop, J., M. H. Stevens, and P. D. Feldman (2007), Molecular nitrogen Carroll-Yoshino  $c'_4$   $^1\Sigma_u^+$   $v' = 0$  emission in the thermospheric dayglow as seen by the Far Ultraviolet Spectroscopic Explorer, *J. Geophys. Res.*, *112*, A10312, doi:10.1029/2007JA012389.
- Boness, M. J. W., and G. J. Schulz (1973), Excitation of high vibrational states of  $N_2$  and CO via shape resonances, *Phys. Rev. A*, *8*, 2883-2886, doi:10.1103/PhysRevA.8.2883.
- Broadfoot, A. L., et al. (1989), Ultraviolet spectrometer observations of Neptune and Triton, *Science*, *246*, 1459-1466.
- Cacciani, P., W. Ubachs, P. C. Hinnen, C. Lynga, and C.-G. Wahlström (1998), Lifetime measurements of the  $E^1\Pi$ ,  $v = 0$  and  $v = 1$  States of  $^{12}\text{C}^{16}\text{O}$ ,  $^{13}\text{C}^{16}\text{O}$ , and  $^{13}\text{C}^{18}\text{O}$ , *Astrophys. J.*, *499*, L223-L226, doi:10.1086/311378.
- Carroll, P. K., and C. P. Collins (1969), High resolution absorption studies of the b-X system of nitrogen, *Can. J. Phys.*, *47*, 563-590, doi:10.1139/p69-073.
- Carroll, P. K., and K. Yoshino (1972), The  $c_n$   $^1\Pi_u$  and  $c'_n$   $^1\Sigma_u^+$  Rydberg states of  $N_2$ : High-resolution studies, *J. Phys. B*, *5*, 1614-1635, doi:10.1088/0022-3700/5/8/025.
- Dixon, W. V., et al. (2007), CalFUSE Version 3: A data reduction pipeline for the Far Ultraviolet Spectroscopic Explorer, *Publ. Astron. Soc. Pac.*, *119*, 527-555.
- Dube, L., and A. Herzenberg (1979), Absolute cross sections from the "boomerang model" for resonant electron-molecule scattering, *Phys. Rev. A*, *20*, 194-213, doi:10.1103/PhysRevA.20.194.
- Edwards, S. A., W.-Ü. L. Tchang-Brillet, J.-Y. Roncin, F. Launay, and F. Rostas (1995), Modelling the VUV emission spectrum of  $N_2$ : Preliminary results on the effects of rotational interactions on line intensities, *Planet. Space Sci.*, *43*, 67-73, doi:10.1016/0032-0633(94)00088-9.
- Eidelsberg, M., J. J. Benayoun, Y. Viala, and F. Rostas (1991), Atlas of the absorption/dissociation spectra of CO and its isotopes between 91.2 nm and 115.2 nm, *Astron. Astrophys. Suppl. Ser.*, *90*, 231-282.
- Feldman, P. D., D. J. Sahnou, J. W. Kruk, E. M. Murphy, and H. W. Moos (2001), High-resolution FUV spectroscopy of terrestrial day airglow with the Far Ultraviolet Spectroscopic Explorer, *J. Geophys. Res.*, *106*, 8119-8129.
- Grimm-Bosbach, T., H. T. Thümmel, R. K. Nesbet, and S. D. Peyerimhoff (1996), Calculation of cross sections for rovibrational excitation of  $N_2$  by electron impact, *J. Phys. B*, *29*, L105-L112, doi:10.1088/0953-4075/29/3/004.

- Haverd, V. E., B. R. Lewis, S. T. Gibson, and G. Stark (2005), Rotational effects in the band oscillator strengths and predissociation linewidths for the lowest  $^1\Pi_u - X^1\Sigma_g^+$  transitions of  $N_2$ , *J. Chem. Phys.*, **123**, 214304, doi:10.1063/1.2134704.
- Helm, H., and P. C. Cosby (1989), Product branching in predissociation of the  $c_4 \ ^1\Pi_u$ ,  $c'_3 \ ^1\Sigma_u^+$ , and  $b^1 \ ^1\Sigma_u^+$  states of  $N_2$ , *J. Chem. Phys.*, **90**, 4208–4215, doi:10.1063/1.455777.
- Helm, H., I. Hazell, and N. Bjerre (1993), Lifetimes and Rydberg-valence state mixing of the  $c'_4 \ ^1\Sigma_u^+$  ( $v = 4$ ) and  $c_3 \ ^1\Pi_u$  ( $v = 4$ ) states of  $N_2$ , *Phys. Rev. A*, **48**, 2762–2771, doi:10.1103/PhysRevA.48.2762.
- James, G. K., J. M. Ajello, B. Franklin, and D. E. Shemansky (1990), Medium-resolution studies of extreme ultraviolet emission from  $N_2$  by electron impact: The effect of predissociation on the emission cross section of the  $b^1\Pi_u$  state, *J. Phys. B*, **23**, 2055–2081, doi:10.1088/0953-4075/23/12/015.
- Joyez, G., R. I. Hall, J. Reinhardt, and J. Mazeau (1973), Low-energy electron spectroscopy of  $N_2$  in the 11.8–13.8 eV energy range, *J. Electron Microscop. Relat. Phenom.*, **2**, 183–190, doi:10.1016/0368-2048(73)80007-6.
- Kam, A. W., J. R. Lawall, M. D. Lindsay, F. M. Pipkin, R. C. Short, and P. Zhao (1989), Precise spectroscopy and lifetime measurement of electron-impact-excited  $N_2$ : The  $c'_4 \ ^1\Sigma_u^+$  ( $v = 3$ ) Rydberg level, *Phys. Rev.*, **40**, 1279–1288, doi:10.1103/PhysRevA.40.1279.
- Kawamoto, Y., M. Fujitake, and N. Ohashi (1997), Near-infrared diode laser spectroscopy of the nitrogen molecule in Rydberg state: Analysis of the  $c_3 \ ^1\Pi_u - a'' \ ^1\Sigma_u^+$ ,  $v = 1-0$  band, *J. Mol. Spectrosc.*, **185**, 330–335, doi:10.1006/jmsp.1997.7404.
- Kransnopolsky, V. A., and P. D. Feldman (2002), Far ultraviolet spectrum of Mars, *Icarus*, **160**, 86–94, doi:10.1006/icar.2002.6949.
- Lefebvre-Brion, H., and R. W. Field (2004), *The Spectra and Dynamics of Diatomic Molecules*, pp. 144, 386–403, Academic, Amsterdam.
- Le Roy, R. J., Y. Huang, and C. Jary (2006), An accurate analytic potential function for ground-state  $N_2$  from a direct-potential-fit analysis of spectroscopic data, *J. Chem. Phys.*, **125**, 164310, doi:10.1063/1.2354502.
- Levelt, P., and W. Ubachs (1992), XUV-laser spectroscopy on the  $c'_4 \ ^1\Sigma_u^+$ ,  $v = 0$  and  $c_3 \ ^1\Pi_u$ ,  $v = 0$  Rydberg states of  $N_2$ , *Chem. Phys.*, **163**, 263–275, doi:10.1016/0301-0104(92)87107-K.
- Lewis, B. R., J. P. England, S. T. Gibson, M. J. Brunger, and M. Allan (2001), Electron energy-loss spectra of coupled electronic states: Effects of Rydberg-valence interactions in  $O_2$ , *Phys. Rev. A*, **63**, 022707, doi:10.1103/PhysRevA.63.022707.
- Lewis, B. R., S. T. Gibson, W. Zhang, H. Lefebvre-Brion, and J. M. Robbe (2005a), Predissociation mechanism for the lowest  $^1\Pi_u$  states of  $N_2$ , *J. Chem. Phys.*, **122**, 144302, doi:10.1063/1.2137722.
- Lewis, B. R., S. T. Gibson, J. P. Sprengers, W. Ubachs, A. Johansson, and C.-G. Wahlström (2005b), Lifetime and predissociation yield of  $^{14}N_2$   $b^1\Pi_u$  ( $v = 1$ ) revisited: effects of rotation, *J. Chem. Phys.*, **123**, 236101, doi:10.1063/1.2137722.
- Lewis, B. R., A. N. Heays, S. T. Gibson, H. Lefebvre-Brion, and R. Lefebvre (2008a), A coupled-channel model of the  $^3\Pi_u$  states of  $N_2$ : Structure and interactions of the  $3s\sigma_g F_3 \ ^3\Pi_u$  and  $3p\pi_u G_3 \ ^3\Pi_u$  Rydberg states, *J. Chem. Phys.*, **129**, 164306, doi:10.1063/1.2990656.
- Lewis, B. R., K. G. H. Baldwin, J. P. Sprengers, W. Ubachs, G. Stark, and K. Yoshino (2008b), Optical observation of  $C$ ,  $F$ , and  $G^3\Pi_u$  states of  $N_2$ , *J. Chem. Phys.*, **129**, 164305, doi:10.1063/1.2990655.
- Liu, X., and D. E. Shemansky (2006), A simple model for  $N_2$  line oscillator strengths of the  $b^1\Sigma_u^+(1)$ ,  $c'_4 \ ^1\Sigma_u^+(0)$ ,  $b^1\Pi_u^e(4)$ ,  $b^1\Pi_u^e(5)$  and  $c_3 \ ^1\Pi_u^e(0) - X^1\Sigma_g^+(0)$  bands, *Astrophys. J.*, **645**, 1560–1566, doi:10.1086/504465.
- Liu, X., D. E. Shemansky, and J. T. Hallett (2005a), The high altitude sunlit Titan ionosphere, *Eos Trans. AGU*, **86**(52), Fall Meet. Suppl., Abstract P33C-0262.
- Liu, X., D. E. Shemansky, M. Ciocca, I. Kanik, and J. M. Ajello (2005b), Analysis of the physical properties of the  $N_2$   $c'_4 \ ^1\Sigma_u^+(0) - X^1\Sigma_g^+(0)$  transition, *Astrophys. J.*, **623**, 579–584, doi:10.1086/428641.
- Liu, X., D. E. Shemansky, C. P. Malone, P. V. Johnson, J. M. Ajello, I. Kanik, A. N. Heays, B. R. Lewis, S. T. Gibson, and G. Stark (2008), Experimental and coupled-channels investigation of the radiative properties of the  $N_2$   $c'_4 \ ^1\Sigma_u^+ - X^1\Sigma_g^+$  band system, *J. Geophys. Res.*, **113**, A02304, doi:10.1029/2007JA012787.
- Meier, R. R. (1991), Ultraviolet spectroscopy and remote sensing of the upper atmosphere, *Space Sci. Rev.*, **58**, 1–186, doi:10.1007/BF01206000.
- Morgan, L. A. (1986), Resonant vibrational excitation of  $N_2$  by low-energy electron impact, *J. Phys. B*, **19**, L439–L445, doi:10.1088/0022-3700/19/11/010.
- Morrison, M. D., C. W. Bowers, P. D. Feldman, and R. R. Meier (1990), The EUV dayglow at high spectral resolution, *J. Geophys. Res.*, **95**, 4113–4127.
- Ndome, H., M. Hochlaf, B. R. Lewis, A. N. Heays, S. T. Gibson, and H. Lefebvre-Brion (2008), Sign reversal of the spin-orbit constant for the  $C^3\Pi_u$  state of  $N_2$ , *J. Chem. Phys.*, **129**, 164307, doi:10.1063/1.2990658.
- Oertel, H., M. Kratzat, J. Imschweiler, and T. Noll (1982), Fluorescence from  $^1\Pi_u$  and  $^1\Sigma_u^+$  states of molecular nitrogen excited with synchrotron radiation between 12.4 and 18.8 eV, *Chem. Phys. Lett.*, **82**, 552–556, doi:10.1016/0009-2614(81)85439-5.
- Ralchenko, Y., F.-C. Jou, D. E. Kelleher, A. E. Kramida, A. Musgrove, J. Reader, W. L. Wiese, and K. Olsen (2007), NIST Atomic Spectra Database (version 3.1.2), Natl. Inst. of Stand. and Technol., Gaithersburg, Md. (Available at <http://physics.nist.gov/asd3>)
- Robertson, A. G., M. T. Elford, R. W. Crompton, M. A. Morrison, W. Sun, and W. K. Trail (1997), Rotational and vibrational excitation of nitrogen by electron impact, *Aust. J. Phys.*, **59**, 441–472.
- Roncin, J.-Y., F. Launay, J.-L. Subtil, and K. Yoshino (1991), New emission bands in the high resolution spectrum of molecular nitrogen between 107.7 and 124.2 nm, *Planet. Space Sci.*, **39**, 1301–1304, doi:10.1016/0032-0633(91)90045-C.
- Roncin, J.-Y., J.-L. Subtil, and F. Launay (1998), The high-resolution vacuum ultraviolet emission spectrum of molecular nitrogen from 82.6 to 124.2 nm: Level energies of 10 excited singlet electronic states, *J. Mol. Spectrosc.*, **188**, 128–137, doi:10.1006/jmsp.1997.7497.
- Roncin, J.-Y., F. Launay, H. Bredohl, and I. Dubois (1999), The vacuum ultraviolet absorption bands of the pink afterglow spectrum of molecular nitrogen revisited at high resolution, *J. Mol. Spectrosc.*, **194**, 243–249, doi:10.1006/jmsp.1998.7773.
- Schultz, G. J. (1964), Vibrational excitation of  $N_2$ , CO, and  $H_2$  by electron impact, *Phys. Rev.*, **135**, A988–A994, doi:10.1103/PhysRev.135.A988.
- Shemansky, D. E., J. M. Ajello, and D. T. Hall (1985), Electron impact excitation of  $H_2$ : Rydberg band systems and benchmark dissociative cross section for H Lyman alpha, *Astrophys. J.*, **296**, 765–773, doi:10.1086/163493.
- Smith, P. L., G. Stark, and K. Yoshino (2003), Laboratory measurements of VUV  $N_2$  photoabsorption cross sections and line widths: Application to planetary-atmospheric transmission models, *Bull. Am. Astron. Soc.*, **35**, 941.
- Spelsberg, D., and W. Meyer (2001), Dipole-allowed excited states of  $N_2$ : Potential energy curves, vibrational analysis, and absorption intensities, *J. Chem. Phys.*, **115**, 6438–6449, doi:10.1063/1.1400139.
- Sprengers, J. P. (2006), Extreme ultraviolet laser excitation of molecular nitrogen: Perturbation and predissociation, Ph.D. thesis, Vrije Univ., Amsterdam. (Available at [http://www.nat.vu.nl/atom/Thesis/Sprengers\\_Thesis.pdf](http://www.nat.vu.nl/atom/Thesis/Sprengers_Thesis.pdf))
- Sprengers, J. P., and W. Ubachs (2006), Lifetimes and transition frequencies of several singlet ungerade states in  $N_2$  between 106,000 and 109,000  $cm^{-1}$ , *J. Mol. Spectrosc.*, **234**, 176–180, doi:10.1016/j.jms.2005.11.001.
- Sprengers, J. P., W. Ubachs, K. G. H. Baldwin, B. R. Lewis, and W.-Ü. L. Tchang-Brillet (2003), Extreme ultraviolet laser excitation of isotopic molecular nitrogen: The dipole-allowed spectrum of  $^{15}N_2$  and  $^{14}N^{15}N$ , *J. Chem. Phys.*, **119**, 3160–3173, doi:10.1063/1.1589478.
- Sprengers, J. P., W. Ubachs, A. Johansson, A. L'Huillier, C.-G. Wahlström, R. Lang, B. R. Lewis, and S. T. Gibson (2004a), Lifetime and predissociation yield of  $^{14}N_2$   $b^1\Pi_u$  ( $v = 1$ ), *J. Chem. Phys.*, **120**, 8973–8978, doi:10.1063/1.1704640.
- Sprengers, J. P., A. Johansson, A. L'Huillier, C.-G. Wahlström, B. R. Lewis, and W. Ubachs (2004b), Pump-probe lifetime measurements on singlet ungerade states in molecular nitrogen, *Chem. Phys. Lett.*, **389**, 348–351, doi:10.1016/j.cplett.2004.03.116.
- Sprengers, J. P., W. Ubachs, and K. G. H. Baldwin (2005a), Isotopic variation of experimental lifetimes for the lowest  $^1\Pi_u$  states of  $N_2$ , *J. Chem. Phys.*, **122**, 144301, doi:10.1063/1.1869985.
- Sprengers, J. P., E. Reinhold, W. Ubachs, K. G. H. Baldwin, and B. R. Lewis (2005b), Optical observation of the  $3s\sigma_g F^3\Pi_u$  Rydberg state of  $N_2$ , *J. Chem. Phys.*, **123**, 144315, doi:10.1063/1.2062189.
- Stahel, D., M. Leoni, and K. Dressler (1983), Nonadiabatic representations of the  $^1\Sigma_u^+$  and  $^1\Pi_u$  states of the  $N_2$  molecule, *J. Chem. Phys.*, **79**, 2541–2558, doi:10.1063/1.446166.
- Stark, G., P. L. Smith, K. P. Huber, K. Yoshino, M. H. Stevens, and K. Ito (1992), Absorption band oscillator strength of  $N_2$  transitions between 95.8 and 99.4 nm, *J. Chem. Phys.*, **97**, 4809–4814, doi:10.1063/1.463835.
- Stark, G., K. P. Huber, K. Yoshino, M.-C. Chan, T. Matusi, P. L. Smith, and K. Ito (2000), Line oscillator strength measurements in the 0-0 band of the  $c'_4 \ ^1\Sigma_u^+ \leftarrow X^1\Sigma_g^+$  transition of  $N_2$ , *Astrophys. J.*, **531**, 321–328, doi:10.1086/308464.
- Stark, G., K. P. Huber, K. Yoshino, P. L. Smith, and K. Ito (2005), Oscillator strength and linewidth measurements of dipole-allowed transitions in  $^{14}N_2$  between 93.5 and 99.5 nm, *J. Chem. Phys.*, **123**, 214303, doi:10.1063/1.2134703.
- Stark, G., B. R. Lewis, A. N. Heays, K. Yoshino, P. L. Smith, and K. Ito (2008), Oscillator strengths and line widths of dipole-allowed transitions

- in  $^{14}N_2$  between 89.7 and 93.5 nm, *J. Chem. Phys.*, *128*, 114302, doi:10.1063/1.2834933.
- Stevens, M. H., R. R. Meier, R. R. Conway, and D. F. Strobel (1994), A resolution of the  $N_2$  Carroll-Yoshino ( $c'_4 - X$ ) band problem in the Earth's atmosphere, *J. Geophys. Res.*, *99*, 417–434.
- Strickland, D. J., R. R. Meier, R. L. Walterscheid, J. D. Craven, A. B. Christensen, L. J. Paxton, D. Morrison, and G. Crowley (2004a), Quiet-time seasonal behavior of the thermosphere seen in the far ultraviolet dayglow, *J. Geophys. Res.*, *109*, A01302, doi:10.1029/2003JA010220.
- Strickland, D. J., J. L. Lean, R. R. Meier, A. B. Christensen, L. J. Paxton, D. Morrison, J. D. Craven, R. L. Walterscheid, J. D. Judge, and D. R. McMullin (2004b), Solar EUV irradiance variability derived from terrestrial far ultraviolet dayglow observations, *Geophys. Res. Lett.*, *31*, L03801, doi:10.1029/2003GL018415.
- Sun, W., M. A. Morrison, W. A. Isaacs, W. K. Trail, D. T. Alle, R. J. Gulley, M. J. Brennan, and S. J. Buckman (1995), Detailed theoretical and experimental analysis of low-energy electron- $N_2$  scattering, *Phys. Rev. A*, *52*, 1229–1256, doi:10.1103/PhysRevA.52.1229.
- Ubachs, W. (1997), Predissociative decay of the  $c'_4$   $^1\Sigma_u^+$ ,  $v = 0$  state of  $N_2$ , *Chem. Phys. Lett.*, *268*, 201–206, doi:10.1016/S0009-2614(97)00179-6.
- Ubachs, W., I. Velchev, and A. de Lange (2000), Predissociation in the  $b$   $^1\Pi_u$  ( $v = 1, 4, 5, 6$ ) levels of  $N_2$ , *J. Chem. Phys.*, *112*, 5711–5716, doi:10.1063/1.481145.
- Ubachs, W., R. Lang, I. Velchev, W.-Ü. L. Tchang-Brillet, A. Johansson, Z. S. Li, V. Lohngyin, and C.-G. Wahlström (2001), Lifetime measurements on the  $c'_4$   $^1\Sigma_u^+$ ,  $v = 0, 1$ , and 2 states of molecular nitrogen, *Chem. Phys.*, *270*, 215–225, doi:10.1016/S0301-0104(01)00378-0.
- van Dishoeck, E. F., M. C. van Hemert, A. C. Allison, and A. Dalgarno (1984), Resonances in the photodissociation of OH by absorption into coupled  $^2\Pi$  states—Adiabatic and diabatic formulations, *J. Chem. Phys.*, *81*, 5709–5724, doi:10.1063/1.447622.
- Vicic, M., G. Poparic, and D. S. Belic (1996), Large vibrational excitation of  $N_2$  by low-energy electrons, *J. Phys. B.*, *29*, 1273–1281, doi:10.1088/0953-4075/29/6/023.
- Vieitez, M. O., T. I. Ivanov, J. P. Sprengers, C. A. de Lange, W. Ubachs, B. R. Lewis, and G. Stark (2007), Quantum-interference effects in the  $o$   $^1\Pi_u$  ( $v = 1$ ) –  $b$   $^1\Pi_u$  ( $v = 9$ ) = 9 Rydberg-valence complex of molecular nitrogen, *Mol. Phys.*, *105*, 134313, doi:10.1080/00268970701291750.
- Vieitez, M. O., T. I. Ivanov, C. A. de Lange, W. Ubachs, A. N. Heays, B. R. Lewis, and G. Stark (2008), Interactions of the  $3p\pi_u$   $c_3$   $^1\Pi_u$  ( $v = 2$ ) Rydberg-complex member in isotopic  $N_2$ , *J. Chem. Phys.*, *128*, 134313, doi:10.1063/1.2883955.
- Walter, C. W., P. C. Cosby, and H. Helm (1993),  $N$  ( $^4S^0$ ),  $N$  ( $^2D^0$ ), and  $N$  ( $^2P^0$ ) yields in predissociation of excited singlet states of  $N_2$ , *J. Chem. Phys.*, *99*, 3553–3561, doi:10.1063/1.466152.
- Walter, C. W., P. C. Cosby, and H. Helm (1994), Predissociation quantum yields of singlet nitrogen, *Phys. Rev. A*, *50*, 2930–2936, doi:10.1103/PhysRevA.50.2930.
- Walter, C. W., P. C. Cosby, and H. Helm (2000), Photoexcitation and predissociation intensities of the  $c'_4$   $^1\Sigma_u^+$  ( $v = 3$  and 4),  $c_3$   $^1\Pi_u$  ( $v = 3$  and 4), and  $b'^1\Sigma_u^+$  ( $v = 10, 12, 13$ , and 15) states of  $N_2$ , *J. Chem. Phys.*, *112*, 4621–4633, doi:10.1063/1.481090.
- Whang, T.-J., G. Zhao, W. C. Stwalley, and C. Y. R. Wu (1996), Franck-Condon factors of the  $b'^1\Sigma_u^+ - X^1\Sigma_g^+$ ,  $c_3$   $^1\Pi_u - X^1\Sigma_g^+$ ,  $c'_4$   $^1\Sigma_u^+ - X^1\Sigma_g^+$ ,  $c'_4$   $^1\Sigma_u^+ - a$   $^1\Pi_g$  and  $o_3$   $^1\Pi_u - X^1\Sigma_g^+$  transitions of  $N_2$ , *J. Quant. Spectrosc. Radiat. Transfer*, *55*, 335–344, doi:10.1016/0022-4073(95)00169-7.
- Yoshino, K., and Y. Tanaka (1977), High-resolution VUV absorption spectrum of  $N_2$ , homogeneous perturbation between  $c'_4$  (0)  $^1\Sigma_u^+$  and  $b'$  (1)  $^1\Sigma_u^+$  levels, *J. Mol. Spectrosc.*, *66*, 219–232, doi:10.1016/0022-2852(77)90212-0.
- Yoshino, K., Y. Tanaka, P. K. Carroll, and P. Mitchell (1975), High resolution absorption spectrum of  $N_2$  in the vacuum-UV region,  $o_{3,4} - X$  bands, *J. Mol. Spectrosc.*, *54*, 87–109, doi:10.1016/0022-2852(75)90011-9.
- Yoshino, K., D. E. Freeman, and Y. Tanaka (1979), High-resolution VUV absorption spectrum of  $N_2$   $c'_4$   $^1\Sigma_u^+ \leftarrow X^1\Sigma_g^+$  bands, *J. Mol. Spectrosc.*, *76*, 153–163, doi:10.1016/0022-2852(79)90224-8.

P. D. Feldman, Department of Physics and Astronomy, Johns Hopkins University, 3400 N. Charles Street, Baltimore, MD 21218-2695, USA. (pdf@pha.jhu.edu)

A. N. Heays and B. R. Lewis, Research School of Physical Sciences and Engineering, Australian National University, Canberra, ACT 0200, Australia. (alan.heays@anu.edu.au; brenton.lewis@anu.edu.au)

X. Liu and D. E. Shemansky, Planetary and Space Science Division, Space Environment Technologies, 320 N. Halstead, Pasadena, CA 91107, USA. (xliu@spacenvironment.net; dshemansky@spacenvironment.net)